Behavior of thin lightly reinforced flat slabs under concentric loading

Ala Torabian[a,b], Brisid Isufi[b], Davood Mostofinejad[a] and António Pinho Ramos[b,c]

[a]Department of Civil Engineering, Isfahan University of Technology (IUT), Isfahan, Iran

[b]Department of Civil Engineering, Faculty of Science and Technology, Universidade NOVA de Lisboa, Caparica, Portugal

[c]CERIS, Lisbon, Portugal

Corresponding author: Ala Torabian; ala.torabian@cv.iut.ac.ir

Abstract

The current research aims to study the behavior of thin reinforced concrete (RC) slabs under concentrated loads as well as to investigate the application of Critical Shear Crack Theory (CSCT) to such slabs. For this purpose, four square 100-mm-thick slabs were cast and subjected to concentrated punching monotonic loading. The experimental parameters were the flexural reinforcement ratio, 0.38% and 1.00%, and the presence or absence of shear headed stud reinforcement. It is shown that the failure criteria of CSCT describe reasonably well the observed failure modes and the ultimate loads of the specimens. However, attention is brought to some peculiarities in the analytical derivation of the load-rotation curve for thin lightly reinforced flat slabs, in which large deformations are experienced. Results showed that in such slabs, the behavior can be highly influenced by the post-yield stress-strain curve of the flexural steel reinforcement. As a result, the constitutive law of steel reinforcement should be explicitly taken into account in such cases. The versatility of CSCT to adapt to these conditions is demonstrated.

Keywords: Critical shear crack theory; punching; thin flat slab; flexural reinforcement ratio; shear headed stud; post-yield.

Declarations of interest: none.

1 Introduction

The use of RC flat slabs for buildings has some advantages over other RC structural systems such as beam supported slabs or slabs with column capitals or drop-down panels. These

advantages include providing more clear space for a given story height and reducing the total height and weight of the building. On the other hand, thin flat slabs suffer from low punching shear capacity and higher deformability. An effective solution for improving the punching shear strength is to employ shear reinforcement around the column, for instance, headed shear studs [1-3] or stirrups [4], which enables the design of thinner flat slabs with higher punching shear capacity, provided that the serviceability limit states are fulfilled. Using shear reinforcement, however, has noticeable effects on the ultimate behavior of flat slabs, which need to be recognized. According to previous researches, ductility of flat slabs can significantly be enhanced by using shear stud reinforcement [1,2]. External shear strengthening of RC slabs using post-installed steel bolts or using fiber-reinforced polymer (FRP) rods, fans, or grids was proved to have similar effects on the slab behavior [5-8].

In two-way RC slabs with no shear reinforcement, the general behavior is highly dependent on the flexural reinforcement ratio. There are several studies in the literature investigating the behavior of two-way slabs with different flexural reinforcement ratios [1, 9-11]. According to them, three general behaviours can be observed based on the amount of flexural reinforcement, as follows:

- The behavior of lightly reinforced slabs is generally ductile, identified by an entire spread of rebars yielding through the full yield-line pattern, deep intrusion of tension cracks, and large plastic deflection of slab prior to failure. Despite the general ductile behavior of such slabs throughout the plastic plateau, the ultimate punching failure remains brittle and leads to a sudden drop in the load carrying capacity of the slab. This type of punching failure is referred to as “flexure-induced punching” [12] and it can lead to an apparent overestimation of the punching shear capacity of lightly reinforced slabs when compared to current code provisions [12]. Yield-line analysis can be used to estimate the capacity of this type of slabs, although the failure loads obtained from the experimental tests are usually larger than the theoretical yield-line, attributed to different causes, e.g. membrane forces, boundary restraints, second-order effects which allow the slab to act as a folded plate, and the neglect of tensile strength of plain concrete [11, 13-15]. While the lightly reinforced slab experiences considerable rotation, a horizontal asymptote is often observed in its load-rotation curve which represents yielding of the entire flexural reinforcement.

- Slabs with medium reinforcement ratio generally fail in a combined flexural-shear failure. Partial yielding of flexural reinforcement occurs in the vicinity of the column and probably along diagonal yield-lines, depending on the level of flexural reinforcement. The lower the reinforcement ratio is, the more the propagation of yielding approaches the full yield-line pattern. In such slabs, punching can occur before yielding of the entire reinforcement at a load level which is lower than the flexural capacity of slab determined by yield-line analysis.
- At high levels of reinforcement, the failure of the slab under concentric loading generally occurs by a brittle punching shear mode, with limited or no yielding of the reinforcement. In this case, the formation of tension cracking prior to the ultimate failure is minimal and the rotation of the slab is relatively small.

The punching shear failure of two-way RC slabs with or without shear reinforcement is a relatively well-studied subject. Accordingly, intense efforts have been made to predict the punching shear capacity of slabs in interior and exterior connections with different characteristics, including different flexural reinforcement ratios, presence or absence of shear reinforcement, and different external strengthening systems.

Based on experimental investigations, design codes present expressions for estimating the punching shear strength of RC slabs, mostly empirical. In most expressions proposed by codes, punching shear strength of slabs without shear reinforcement is defined as a function of concrete compressive strength, slab thickness, column size, and flexural reinforcement ratio. The expressions proposed by ACI 318 [16] and Eurocode 2 [17] are presented in Table 1. The basic ACI 318 provision for punching capacity has not changed since 1963 and is independent of the reinforcement ratio [16]. On the other hand, the punching shear strength provision of Eurocode 2, which is based on Model Code 1990 [18], is depended on the flexural reinforcement ratio [17]. Formulations to evaluate the punching shear capacity of slabs reinforced with different types of punching shear reinforcement can also be found in codes of practice. Crushing of the concrete struts in the vicinity of the column, punching within the shear-reinforced slab zone, and punching outside this zone are the failure modes that are considered in the codes. Criteria or expressions are presented by codes to consider the strength of the slab corresponding to each of the above-mentioned failure modes, and the minimum strength specifies the governing failure mode of the slab.

90 Table 1 ACI 318 and Eurocode 2 expressions for punching shear

Code	Expressions
ACI 318 [16]	$v_c = \min \begin{cases} 0.33\sqrt{f_c} \\ 0.17(1+\frac{2}{\beta})\sqrt{f_c} \\ 0.083(\frac{\alpha_s d}{b_0}+2)\sqrt{f_c} \end{cases}$ where f_c is the specified compressive strength of concrete β is the ratio of long to short sides of the column α_s is 40, 30, and 20 for an interior, edge, and corner column, respectively d is the effective depth of slab b_0 is the perimeter length of the critical section assumed at a distance $0.5d$ from the column edge
Eurocode 2 [17]	$v_c = (0.18/\gamma_c)k(100\rho f_{ck})^{1/3} \geq v_{min}$ where $k = 1 + \sqrt{200/d} \leq 2.0$ γ_c is the partial factor for concrete f_{ck} is the characteristic compressive strength of concrete at 28 days $\rho = \sqrt{\rho_y \cdot \rho_z} \leq 0.02$ ρ_y and ρ_z are the ratios in two perpendicular y and z directions, respectively. ρ_y and ρ_z are calculated as mean values considering a slab width equal to the column width plus $3d$ each side. $v_{min} = 0.035k^{3/2}{f_{ck}}^{1/2}$

91 One of the most comprehensive approaches to describe the behavior of flat slabs under
92 concentric loading is the Critical Shear Crack Theory (CSCT). The fundamentals of the
93 theory were first presented by Muttoni and Schwartz [19], based on earlier work by Kinnunen

and Nylander [20], according to which- for structural elements without shear reinforcement- "a critical shear crack" propagating through the strut that carries the shear force to the column is responsible for the punching shear failure and that the punching resistance is a function of slab's rotation outside the critical shear crack. In Muttoni [21], the theory was completed by including a failure criterion and a code-like formulation for the punching shear design of flat slabs (refer to Section 2 for details). The application of CSCT for punching shear-reinforced slabs was later extended by Ruiz and Muttoni [22] (refer to Section 2). Afterwards, the CSCT was extended to different types of flat slabs by several researchers. Clément et al. [23, 24] proposed its application to prestressed slabs. In 2014, Faria et al. [25] extended the application of CSCT to slabs strengthened with FRP composites, by proposing changes to the analytical derivation of the load-rotation curve as well as changes in the failure criterion resulting from the application of FRP. Lapi et al. [26] demonstrated the versatility of CSCT by applying it to flat slabs strengthened with a reinforced concrete overlay. A review and summary of the work related to the extension of CSCT to various punching shear strengthening techniques are presented in Lapi et al. [27].

In the current study, relatively thin slabs (with depth 100 mm) with and without shear studs are tested under concentric punching shear load and the experimental results are compared with CSCT predictions. Two different flexural reinforcement ratios are considered, 0.38% and 1.00%. The present study sheds light on the applicability of CSCT in extreme cases (thin slabs and low flexural reinforcement) and contributes towards the completeness of the theory. In practice, the low flexural reinforcement ratio can be found in cases of high corrosion of steel reinforcement or deficient initial design, for instance. The low thickness can represent a deficient initial design in an existing structure or a poorly executed slab with a concrete cover higher than the designed one. It should be noted that the main body of work on which the CSCT theory is calibrated refers to interior slab-column connections; therefore, this study focuses on internal slab-column connections to extend this theory in the above-mentioned conditions.

2 Critical Shear Crack Theory

2.1 Description

An illustration of the application of CSCT is given in Fig. 1. According to the theory, punching failure occurs at the intersection of the load-rotation curve with the failure criterion.

The load-rotation curve can be constructed using a nonlinear finite element analysis or analytically for simple cases. The analytical solution for axisymmetric slabs is obtained by dividing the slab into sector elements extended from the critical shear crack (located at a radius $r_0=r_c+d$, where r_c is the radius of the column, assumed circular and d is the slab's effective depth) to a radius equal to the radius of the hogging moment region of the slab. It is assumed that the slab rotation, ψ, is constant outside the critical shear crack. Inside the radius r_0, the radial and tangential moments are assumed constant and the radial curvature is assumed to be equal to the tangential curvature. Internal forces are then calculated assuming a quadrilinear moment-curvature relationship and the equilibrium conditions of the sector elements are used to calculate the shear force, V, for a given slab rotation, ψ [21].

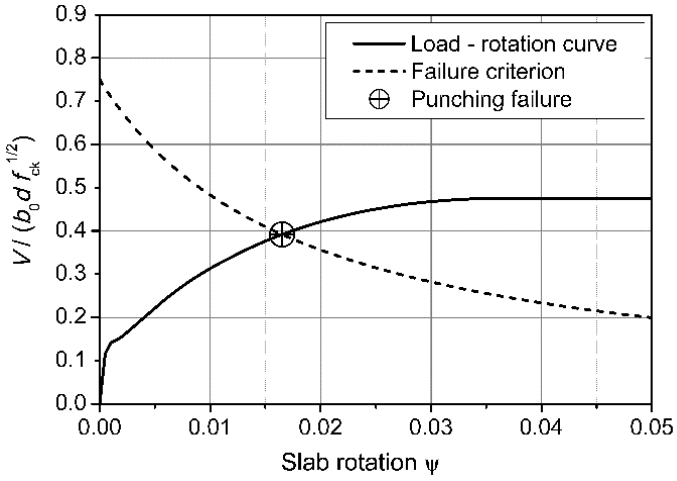

Fig. 1. Example of application of CSCT for a slab-column connection without shear reinforcement

For the construction of the load-rotation curve, Muttoni [21] also proposed a simplified formulation based on the assumption that the load-rotation curve up to the flexural strength V_{flex} follows a parabola with an exponent equal to 3/2:

$$\psi = 1.5\frac{r_s f_y}{dE_s}\left(\frac{V}{V_{flex}}\right)^{3/2} \quad (1)$$

where, ψ is the slab rotation, r_s is the radius of the slab (which, in the simplified approach can be assumed equal to the radius of the zero moments line), f_y is the steel yield stress, d is the effective depth of the slab, E_s is the modulus of elasticity of steel and V is the applied shear force.

Based on a semi-empirical formulation, assuming crack width proportional to the slab rotation (ψ) and effective depth (d) as well as taking into account the roughness of the crack, the failure criterion (Fig. 1) for slabs without shear reinforcement is expressed as follows [21]:

$$\frac{V}{b_0 d\sqrt{f_c}} = \frac{3/4}{1+15\dfrac{\psi d}{d_{g0}+d_g}} \tag{2}$$

where, b_0 is the control perimeter, taken at a distance $d/2$ from the face of the column; d_g is the maximum aggregate size and d_{g0}=16 mm is a reference aggregate size.

Ruiz and Muttoni [22] extended the application of CSCT to the design of flat slabs with shear reinforcement. In this case, the load-rotation relationship is assumed to be the same as in slabs without shear reinforcement, because it only depends on the flexural properties of the slab. For slabs with shear reinforcement, failure can occur through the shear reinforcement, outside the shear-reinforced zone or near the face of the column due to the crushing of concrete (Fig. 2). The resistance for each of these three failure modes is determined at the intersection of the load-rotation curve with the corresponding failure criteria.

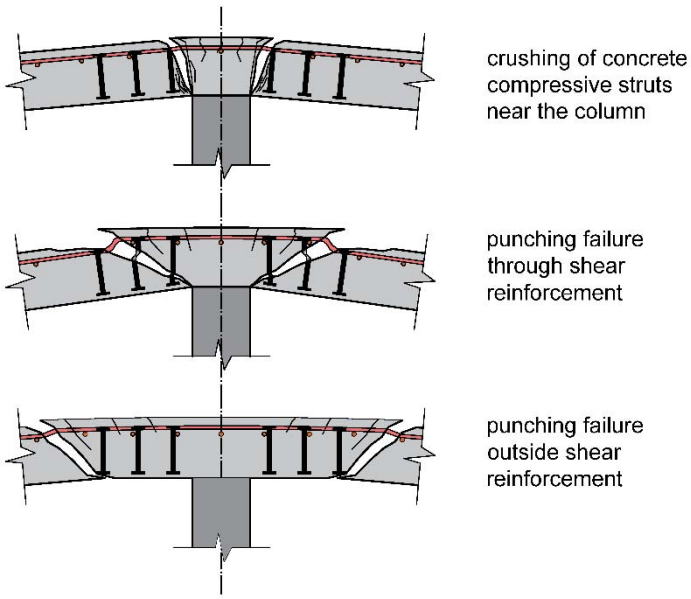

Fig. 2. Possible punching failure modes for slabs with punching shear reinforcement

160 The criterion for failure within the shear-reinforced zone is based on a simple mechanical
161 model consistent with CSCT, which considers the stress and bonding conditions in each shear
162 reinforcement leg. In contrast to the provisions of major design codes [16, 17], the
163 contribution of shear reinforcement is not considered constant for all levels of slab rotation in
164 CSCT [22].

165 The failure criterion for punching outside the shear reinforcement is calculated as in case of
166 slabs without shear reinforcement, but with an adapted perimeter (taken at a distance $d/2$
167 from the outermost shear reinforcement units) and with a reduced effective depth. This
168 accounts for the geometry of the crack outside the shear-reinforced zone due to pull-out of
169 shear reinforcement as a block [22].

170 Equations for the failure due to the crushing of concrete near the column are also provided in
171 Ruiz and Muttoni [22]. In this case, the right-hand side of Equation (2) is multiplied by a
172 factor λ equal to 3.0 for headed studs and 2.0 for other types of shear reinforcement. The
173 control perimeter is taken at a distance d/2 from the edges of the column.

174 **2.2 Experimental validation of CSCT**

175 CSCT for flat slabs without shear reinforcement was validated in Muttoni [21] against 87
176 experiments of isolated slab-column connections under monotonic concentric loading. The
177 failure criterion was based on a slightly larger database of 99 specimens. The database of
178 tests used in Muttoni [21] to validate the CSCT contained slabs with an effective depth
179 ranging from 96 mm to 464 mm.

180 An experimental campaign addressing specifically the behavior of flat slabs with low
181 amounts of flexural reinforcement was presented in Guandalini et al. [28]. In total, 11
182 specimens were tested under concentric loading, with a longitudinal reinforcement ratio
183 varying from 0.22% to 1.50% and slab thickness from 125 mm to 500 mm. Two of the
184 specimens, named PG-8 and PG-9 in Guandalini et al. [28], were both thin (thickness equal to
185 only 125 mm) and lightly reinforced (with a longitudinal ratio equal to 0.28% and 0.22%
186 respectively). In these two specimens, punching failure occurred after relatively large plastic
187 rotation of the slab. The experimental results of the 11 specimens fitted well with the failure
188 criterion of CSCT. Guandalini et al. [28] also reported a lightly reinforced thick slab
189 (thickness 500 mm). The thick lightly reinforced slab did not exhibit full yielding of the

flexural reinforcement and prematurely failed in punching in contrast to observations on lightly reinforced thin slabs. CSCT predicted reasonably well the behavior of this specimen.

The extension of CSCT proposed in Ruiz and Muttoni [22] for shear-reinforced flat slabs was validated against 45 concentric punching tests. In the database used by the authors [22], 19 of the tests contained studs (either with smooth or deformed shaft). The effective depths of the specimens varied from 124 mm to 350 mm.

Further verification of CSCT is presented in Einpaul et al. [29], where it was shown that CSCT considers the influence of slab slenderness in a consistent manner and gives better results compared to EC2 [17] and ACI 318 [16] codes. The 13 specimens reported in Einpaul et al. [29] and 21 additional ones from the literature had an effective depth from 118 mm to 218 mm. Three of the specimens contained shear reinforcement.

3 Experimental campaign

3.1 Experiment preparation and test scheme

Four RC slabs of 1.85×1.85×0.1 m were constructed and tested as simply supported at their perimeter with corners free to lift, whereas the effective flexural span was 1.7 m. The tests were carried out in structural laboratory of Isfahan University of technology (IUT). A layout of the tested slabs is shown in Fig.3, which also shows the specimens' flexural reinforcement details. Two different reinforcement ratios of 0.38% and 1.00% were used. The clear concrete cover to the flexural rebars was set as 20 mm in all specimens. The specimens were cast upside-down, meaning that the flexural reinforcement was placed next to the bottom of the mould; therefore, proper control over the effective depth was possible. It should be mentioned that since thin slabs are sensitive to construction tolerances, the locations of flexural and shear reinforcement were properly adjusted in the mould; moreover, accurate measurements of the effective depth were taken during casting as well as after testing.

Two of the test specimens were reinforced with a total of 12 shear stud rails with 8 layers. The shear stud reinforcement was designed according to punching shear principles of ACI 318 and Eurocode 2 such that the shear reinforced specimens could reach their flexural capacity before they fail in punching. The shear reinforcement arrangement is shown in Fig.4. The available shear studs, with a shaft diameter of 19 mm and overall head diameter of 32

mm, were welded to an 8-mm-thick rail with a spacing of 55 mm using a stud welding gun based on ASTM A1044 criteria [30]. Studs with such large shaft diameter were employed for economic purposes since they were the only available studs in the local market, and the available stud welding gun only fitted this size of the shaft. The diameter of the bearing surface of the head was 30 mm. Based on ASTM A1044 [30] and ACI 318 [16], the area of the head of headed shear studs is required to be at least 10 times the area of the shaft. Accordingly, the effective diameter of the shaft was calculated as 9.5 mm fulfilling this requirement considering the provided head bearing area. It should be noted that the effective diameter was sufficient for the aim of this study since the purpose of employing the shear studs was hindering occurrence of punching failure before achieving the flexural capacity; and yielding of the studs was not aimed in this study. The stud rails were placed into the mould such that the distance between the first row of studs and the column face was 30 mm. The designation of the specimens along with a summary of their characteristics is presented in Table 2.

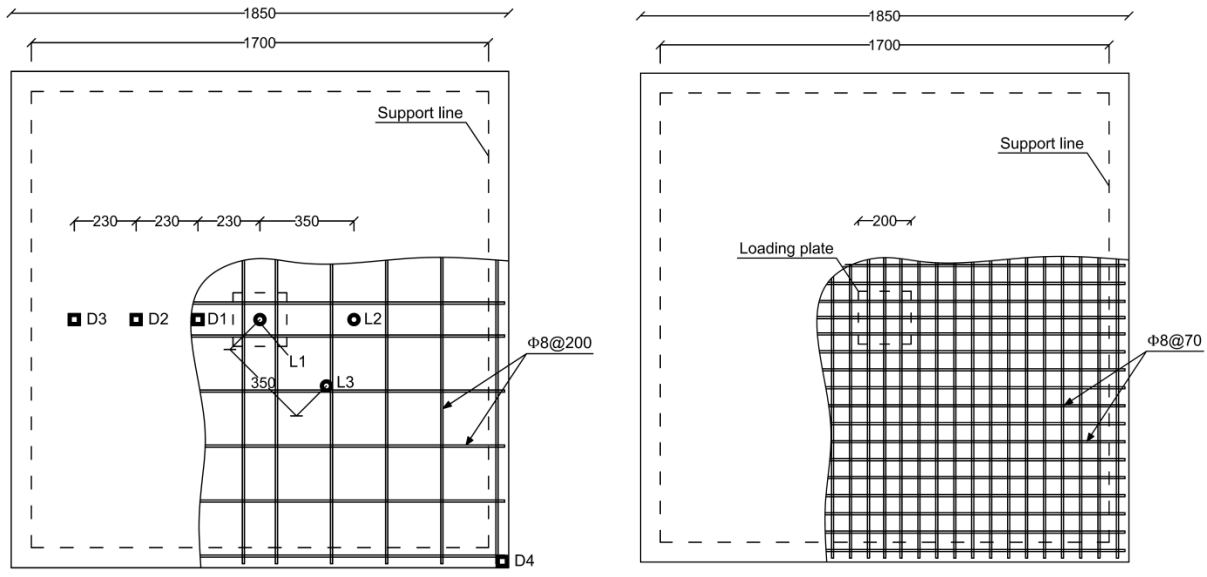

Fig.3. Layout of test specimens and flexural reinforcement details (dimensions are in mm, L1-L3 refer to LVDTs, and D1-D4 refer to dial gauges); (a) specimens with reinforcement ratio of 0.38%; (b) specimens with reinforcement ratio of 1.00%

The compressive strength of the concrete used for the construction of specimens was measured on average as 42 MPa by carrying out compression tests on 150×300 mm cylindrical concrete samples in accordance with ASTM C39 [31]. The values for each

specimen are given in Table 2. The aggregates employed in the concrete included 5-12 mm coarse aggregates and 0-5 mm sand. According to standard tensile tests conducted on steel bars, the yield and ultimate strength of the employed rebars were 450 and 700 MPa, respectively. Tensile strength and yield strength of shear studs were respectively 450 MPa and 350 MPa, based on the data reported by the manufacturer.

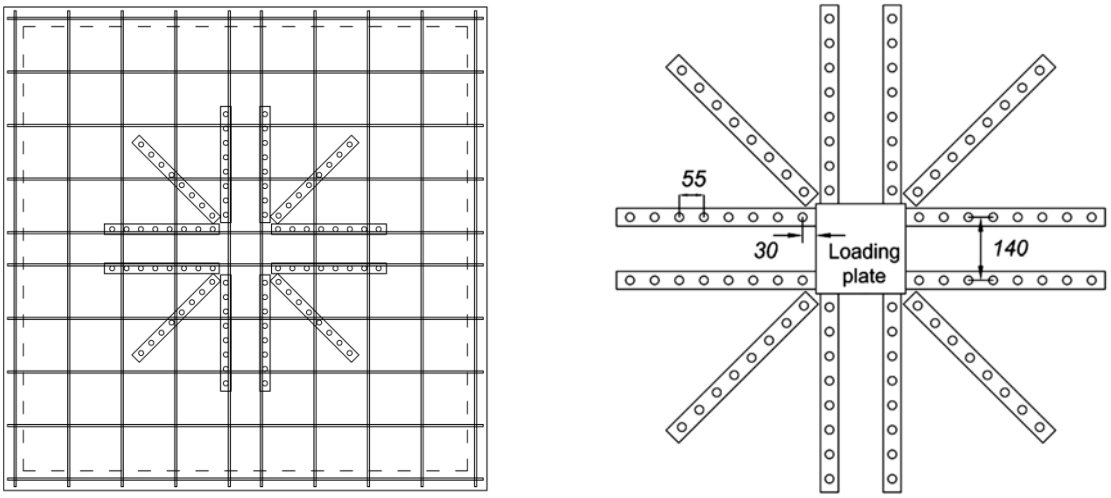

(a) (b)

Fig.4. Arrangement of shear studs in shear reinforced specimens (dimensions in mm); (a) position of shear studs with respect to the flexural reinforcement; (b) close-up of shear reinforcement

Table 2 Summary of specimens' characteristics and test results

Specimen	Concrete strength f_c (MPa)	Flexural reinforcement ratio (%)	Punching shear reinforcement	Failure load (kN)	Ultimate rotation (rad)
US-0.38	43.0	0.38	Unreinforced	101.6	0.075
US-0.38-stud	41.7	0.38	Shear studs	117.1	>0.189*
US-1.00	41.9	1.00	Unreinforced	186.3	0.035
US-1.00-stud	42.2	1.00	Shear studs	224.0	0.100

* Exact ultimate rotation was not measured due to limitations of the instruments, but it was only marginally larger than the shown value

The specimens were tested using a reaction steel frame and the load was applied in the center of the slab over an area of 200×200 mm^2 (Fig.5).The load was measured by an external load cell. Two linear variable differential transducers (LVDTs), L1-L2, and three dial gauges, D1-D3, were installed along the width of the specimen with the arrangement shown in Fig.3. One LVDT, L3, and one dial gauge, D4, were also placed along the diagonal direction of the specimen: L3 at a distance of 350 mm from the central LVDT and D4 on top of the slab corner (Fig.3).

Fig.5. Reaction frame and test setup

3.2 Experimental results

3.2.1 Deflections and load-rotation behavior

Fig.6 demonstrates the deflected shapes of the test specimens along their width for varying load levels, which were obtained by measurements of the installed LVDTs and dial gauges. According to CSCT, the deflected shape of the slab is conical outside the critical shear crack, meaning that the rotation ψ of the slab can be considered constant in this region [21]. The experimental results in the current study also confirm this claim, as the deflection profile of each specimen represents a nearly conical shape of the deflected specimen (Fig.6).

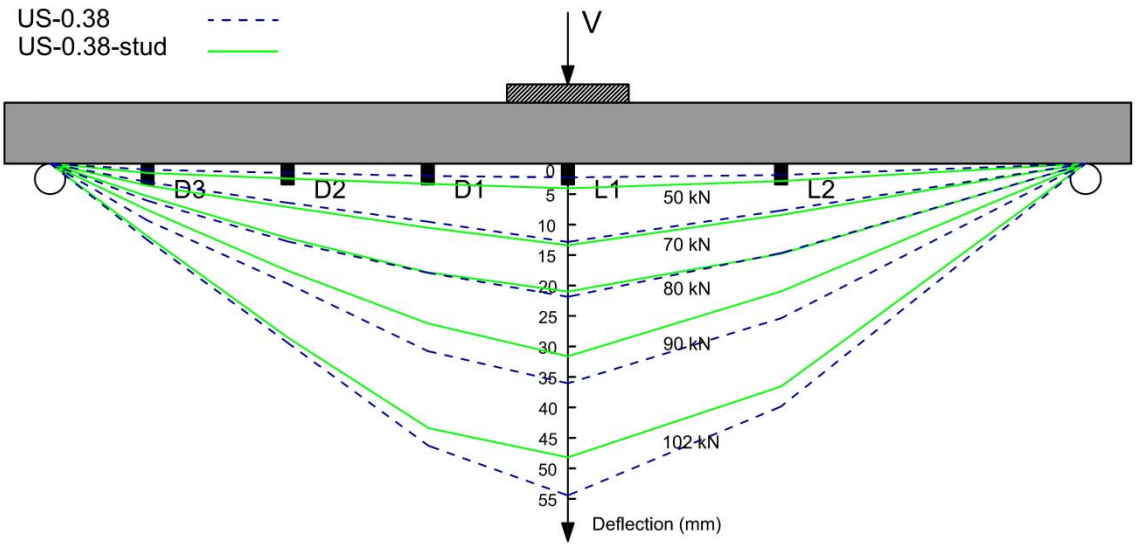

(a)

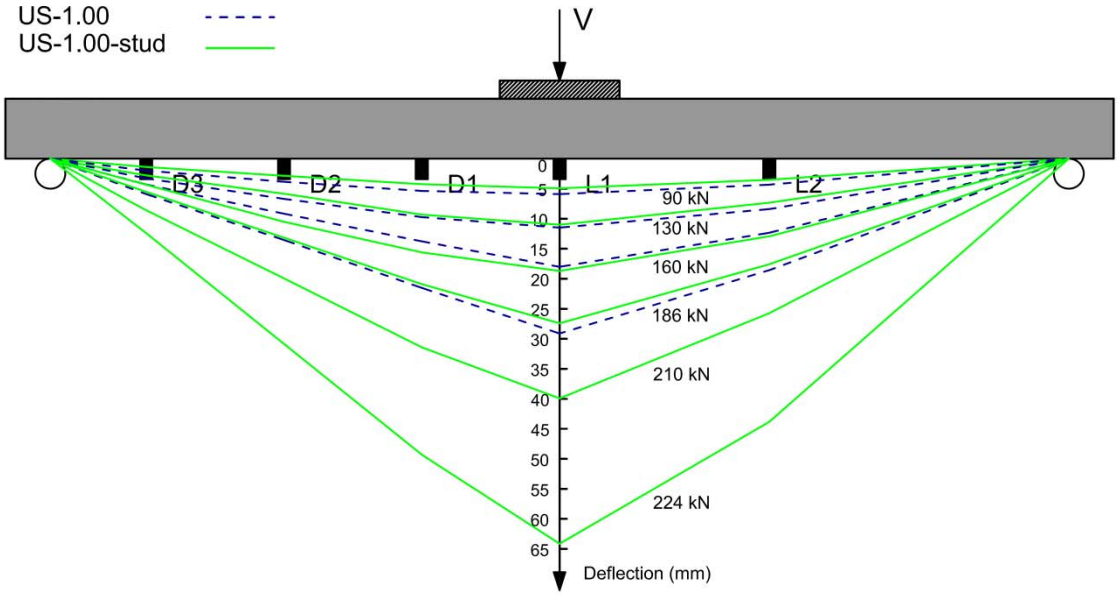

(b)

Fig.6. Deflection profiles; (a) specimens with reinforcement ratio of 0.38%; (b)specimens with reinforcement ratio of 1.00%

The load-rotation curves of all the tested specimens are presented in Fig.7. The slab's rotation at each load level was computed using the deflection profile outside the critical shear crack, considering as the angle of the deformed shape of the slab upward from the undeformed shape in this region. After a linear elastic branch, flexural cracking decreases the stiffness of

the specimens, which is then remarkably dependent on the flexural reinforcement ratio. As it can be observed in Fig.7, the post-cracking stiffness of the specimens with low reinforcement ratio (0.38%) is much lower than that of the specimens with 1.00% flexural reinforcement. In lightly reinforced specimens with relatively small slab depths, large deflections are experienced due to the spread of steel yielding while a plastic plateau can be observed. In cases that the flexural steel reinforcement reaches the strain hardening region of the stress-strain curve, the load capacity is gently increased while considerable deflection is experienced. The post-cracking behavior of specimens with large deflections is therefore influenced by the stress-strain curve of the flexural reinforcement.

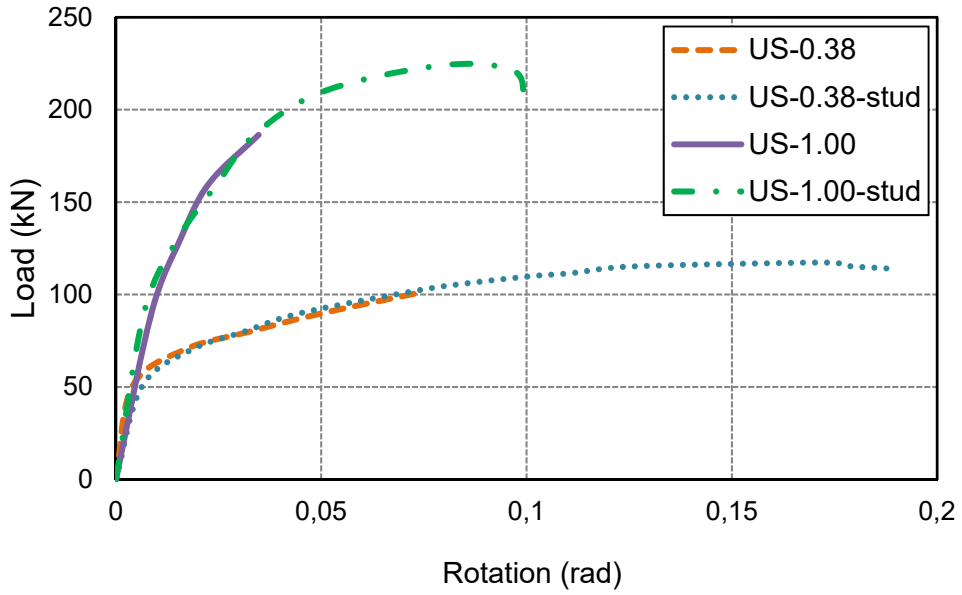

Fig.7. Load-rotation curves of specimens

The deflection profiles of the specimens along half of their diameter were obtained using the measurements of the LVDTs L1 and L3 and the dial gauge D4 (see Fig. 3). Fig. 8 shows these profiles at different load levels. Accordingly, the distance between the central point and the zero-deflection point was around 0.9 m.

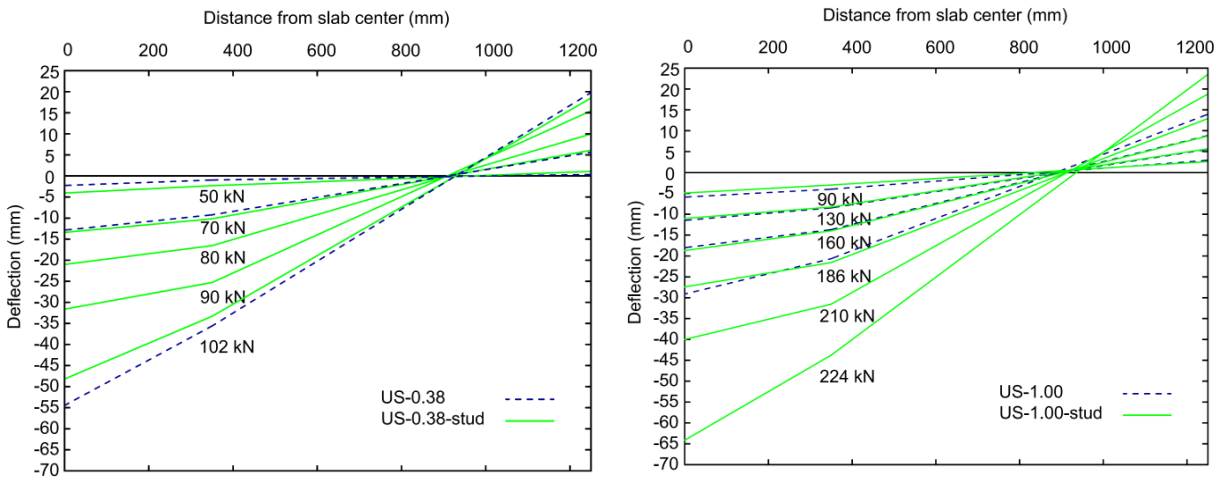

(a) (b)

Fig. 8. Deflection profiles along diagonal direction of specimens; (a) specimens US-0.38 and US-0.38-stud; (b) specimens US-1.00 and US-1.00-stud

3.2.2 Cracking and failure modes

Fig.9 demonstrates the tension and compression faces of the tested specimens after failure. The final failure mode for all specimens was punching shear. The behavior of each specimen before ultimate failure was strongly influenced by the flexural reinforcement ratio as well as the presence of shear reinforcement. In specimens US-0.38 and US-0.38-stud, radial flexural cracks propagated in the tension face of the slab. By increasing the applied load, the propagation and width of the cracks increased, yielding of the flexural reinforcement approached the full yield-line pattern, and consequently, the slab experienced large plastic deflections. Afterward, punching shear failure as the ultimate failure mode led to an abrupt load drop. In specimen US-0.38, punching failure happened with a clearly delimited punching cone (Fig.9a), and specimen US-0.38-stud experienced punching failure outside the shear stud reinforcement. In the specimens with a reinforcement ratio of 1.00%, the behavior of the slab was dependent on the existence of shear studs. In specimen US-1.00, hairline flexural cracks with limited propagation formed, and then abrupt punching shear failure occurred. In specimen US-1.00-stud, however, a significant spread of flexural cracks in the radial direction was observed, and then the ultimate punching failure occurred outside the shear studs after large deformation of the slab (Fig.9d). The general behavior and mode of failure of shear stud reinforced specimens show that the employed studs reinforcement worked properly although the provided anchorage was less than the anchorage required by

309 ACI 318 [16]. Indeed, as mentioned before, the provided anchorage for the studs is sufficient
310 for shaft diameter of 9.5 mm according to ACI 318 [16], which satisfies the required area of
311 shear reinforcement to resist punching shear failure inside the shear reinforcement.

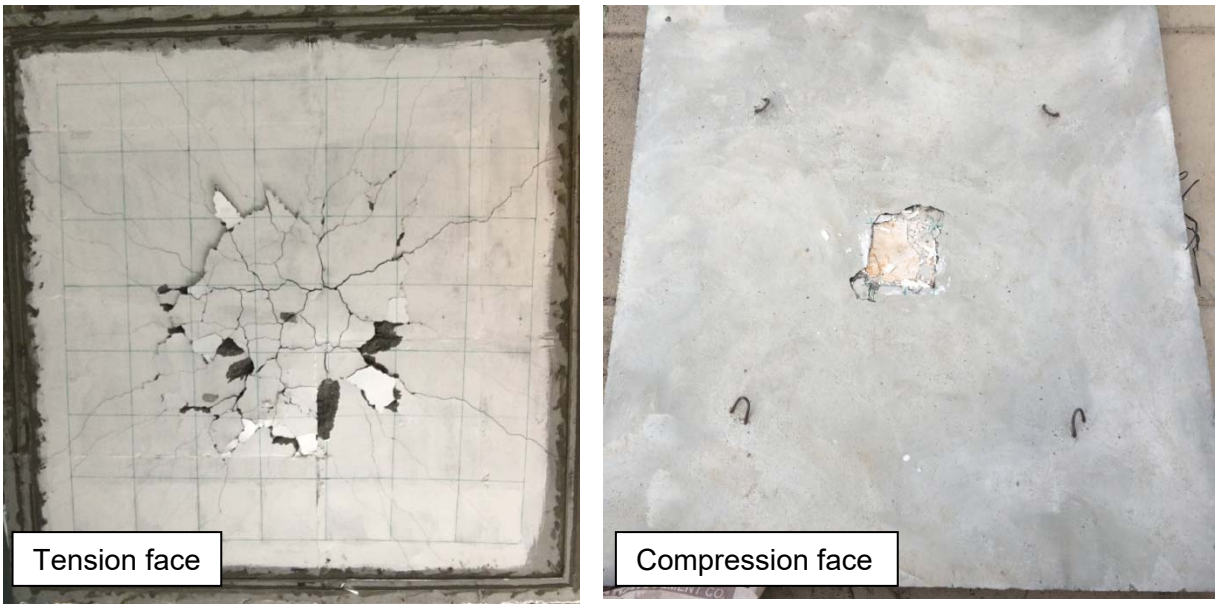

(a)

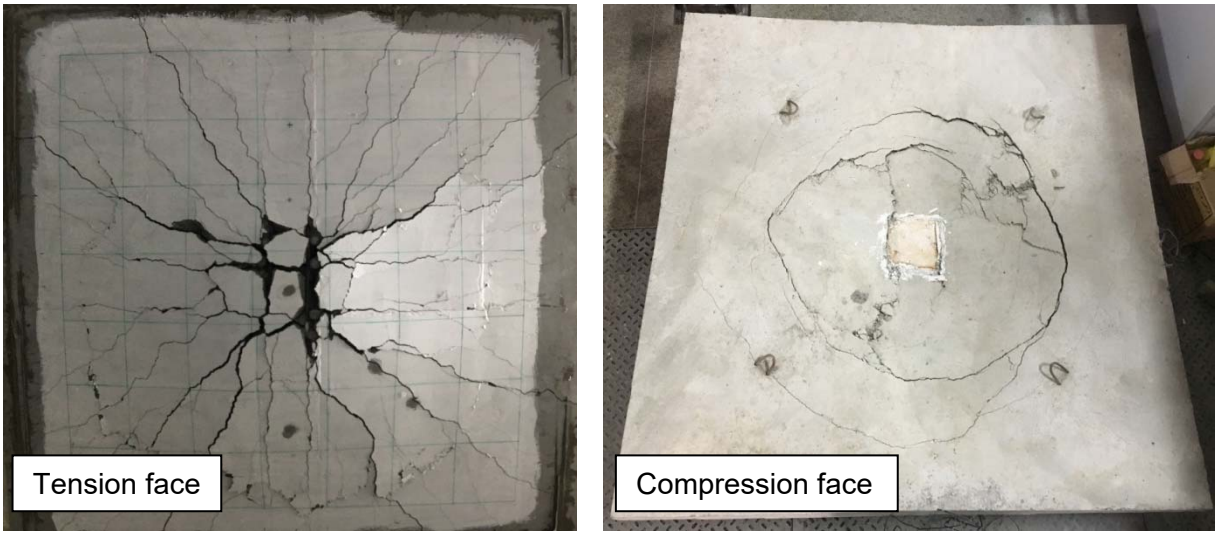

(b)

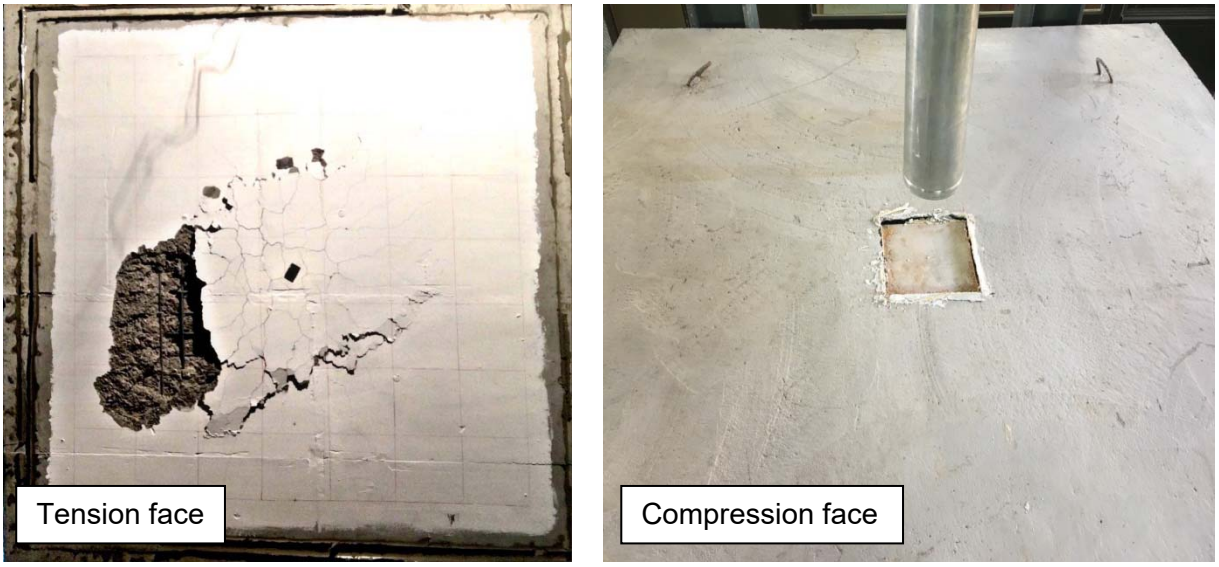

(c)

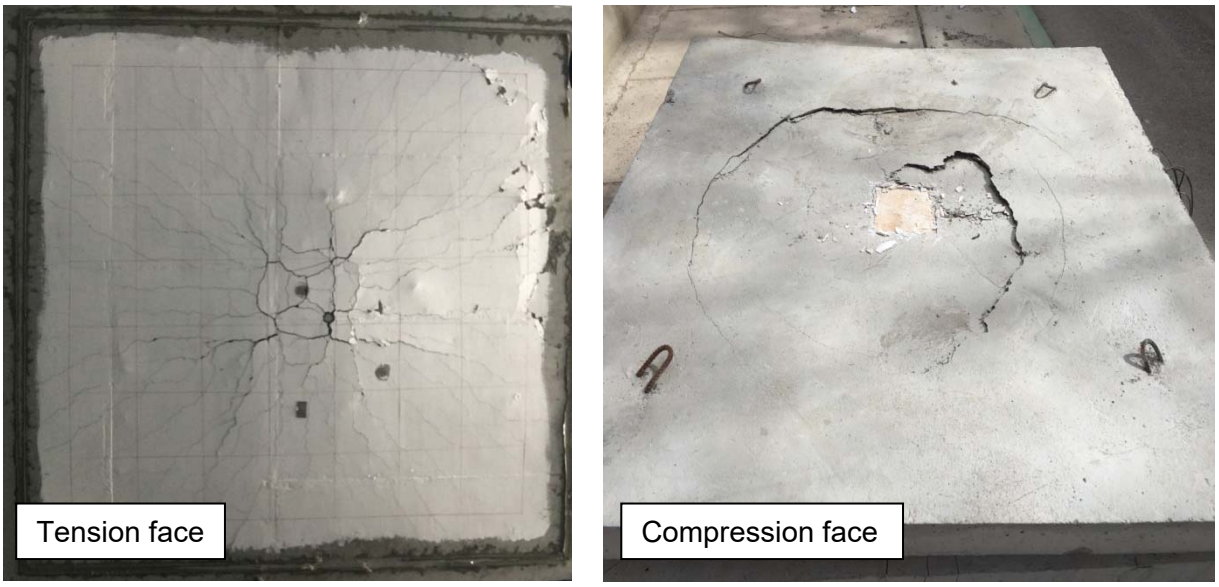

(d)

Fig.9. Specimens after failure; (a) specimen US-0.38; (b) specimen US-0.38-stud; (c) specimen US-1.00; (d) specimen US-1.00-stud

3.2.3 Effect of shear reinforcement

The values of the failure load and ultimate rotation of the specimens are presented in Table 2. Referring to these values and the load-rotation curves in Fig.7, it can be concluded that using shear stud reinforcement leads to an enhancement of the load-bearing capacity of the slab as well as an increase of its ultimate rotation. In fact, as can be observed in Fig.7, the specimen

with shear studs behaved similarly to the specimen with no shear reinforcement up to the maximum load level of the later, in accordance with the assumption presented by Ruiz and Muttoni [22] for the extension of CSCT to shear-reinforced flat slabs.

In lightly reinforced specimens (US-0.38 and US-0.38-stud), utilizing shear studs did not change the mode of failure as in both tests full yield-line pattern and flexural cracks formed and then the slab finally failed in punching. However, shear reinforcement considerably increased the ultimate rotation from 0.075 rad in specimen US-0.38 to more than 0.189 rad in specimen US-0.38-stud. The load capacity of specimen US-0.38-stud was 117.1 kN while the maximum load in specimen US-0.38 was 101.6 kN. This 15% improvement in load capacity is due to the effectiveness of shear studs in postponing the punching shear failure. In specimens with higher reinforcement ratio (US-1.00 and US-1.00-stud), the employment of studs considerably influenced the general behavior of the slabs: specimen US-1.00 failed abruptly in punching after limited formation of hairline flexural cracks, while specimen US-1.00-stud failed in a much more ductile manner since flexural steel bars were allowed to reach higher strains, causing a plastic plateau in the load-rotation curve after which the ultimate punching failure occurred. Accordingly, the failure load in US-1.00 and US-1.00-stud was measured as 186.3 and 224.0 kN, respectively, showing an increase of 20%. It should be noted that the increase in failure load due to the application of studs in the present tests was relatively small when compared to tests available in the literature because the maximum load carried by the specimens was limited by their flexural capacity, as discussed in detail in Section 4. Ultimate rotation also increased from 0.035 rad in specimen US-1.00 to 0.1 rad in specimen US-1.00-stud as a result of using shear reinforcement.

4 Comparison of experimental results with CSCT

4.1 Peculiarities of thin lightly reinforced flat slabs

The specimens described in Section 3 are relatively thin. They are thinner than the specimens described in Section 2.2 in publications with which CSCT was validated. Nevertheless, these experimental results serve to check the applicability of the CSCT failure criterion and of the load-rotation curve based on the CSCT assumptions for such extreme conditions.

When the slab is thin and lightly reinforced, it can deflect considerably before punching failure, as it was observed in Section 3 for specimen US-0.38-studs. Due to the large slab rotation, ψ, the strains in the longitudinal steel bars can become very large. The strain

hardening region of the stress-strain curve of the longitudinal reinforcement steel is therefore expected to significantly influence the load-rotation curve of such specimens. The effect of the post-yielding curve of the longitudinal reinforcement steel is further accentuated for the specimens described in this paper by the fact that the longitudinal steel bars exhibited a relatively short yielding plateau, as shown in Fig. 10. The influence of the post-yield behavior of the longitudinal reinforcement steel in the flexural capacity as determined by a yield-line analysis is demonstrated in Table 3.

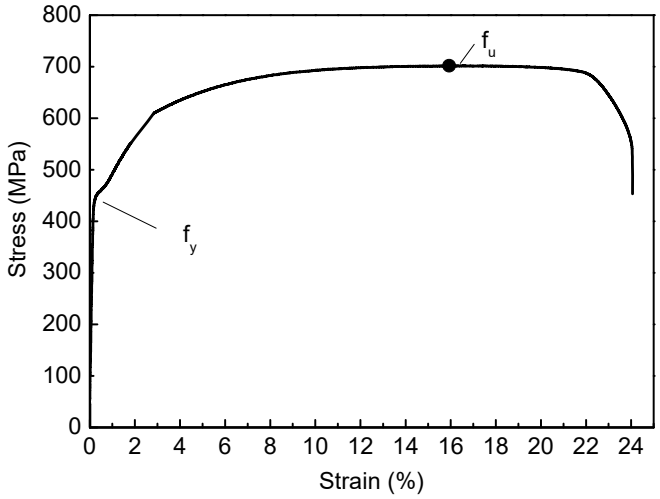

Fig. 10. Stress-strain relationship for the longitudinal steel bars used in the experimental campaign

Table 3. Effect of strain hardening on the flexural capacity

Flexural reinforcement ratio (%)	f_y (MPa)	f_u (MPa)	$V_{flex,y}$ (kN)	$V_{flex,u}$ (kN)	$V_{flex,u}/V_{flex,y}$
0.38	450	700	73.7	106.3	1.44
1.00	450	700	190.4	224.7	1.18

Fig. 11 illustrates the conditions of support and loading as well as the yield-line pattern in the current study. In this figure, l_s, l_l, and c are the slab side length, the distance between the supports and the column size, respectively. As shown in the figure, the slab corners are permitted to lift by rotation about axes at 45 degrees. These conditions cause the formation of circumferential yield lines around the column and diagonal yield lines intersecting the support lines at a distance l_{up} shown in Fig. 11[11, 32, 33]. Based on Elstner and Hognestad [11], l_{up} can be approximately estimated as $(1-\sqrt{2}/2)(l_l-c)$. Accordingly, the value of l_{up} would

be approximately 440 mm for the conditions in this study. Considering the slabs' geometry, this value is compatible with the deflection of the slab along its diagonal described in Section 3.2.1 and shown in Fig. 8. Further verification of the yield-line pattern is provided in Section 5.2.

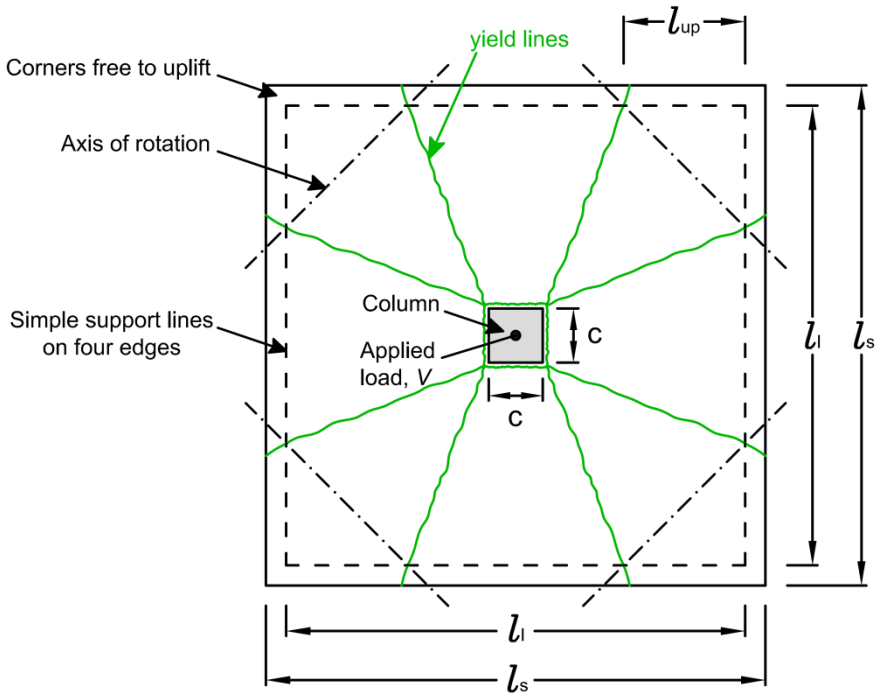

Fig. 11. Support and loading conditions and yield-line pattern

In Table 3, the yield stress is denoted as f_y. The ultimate steel stress, i.e., considering strain hardening is denoted as f_u. The flexural capacity $V_{flex,y}$ is calculated assuming steel stress f_y, whereas the ultimate flexural capacity, $V_{flex,u}$ is calculated assuming a compressive strain equal to 0.38% for concrete and a nonlinear stress-strain curve for steel in accordance with Fig. 10. The table shows that the ratio between $V_{flex,u}$ and $V_{flex,y}$ in the specimen with flexural reinforcement ratio of 0.38% and 1.00% is 1.44 and 1.18, respectively. Table 3 reveals that the influence of the post-yield behavior of steel in the flexural capacity is significant for both cases but it is more significant for the specimens with low reinforcement ratio.

4.2 Moment-curvature relationships

For simple cases, Muttoni [21] proposes the use of a quadrilinear moment-curvature relationship for the slab section (Fig. 12, using symbols from Muttoni [21]), to be used in the formulation of equilibrium equations for the construction of the load-rotation curve in

accordance with the assumptions of CSCT. For the reasons described in Section 4.1, the slab load-rotation curve is expected to deviate significantly from the experimental one if the post-yield stress-strain relationship of the longitudinal reinforcement steel is not taken into account.

To account for the post-yield behavior of the longitudinal reinforcement steel, the moment-curvature relationship of the slab section was constructed considering the actual stress-strain relationship of steel from Fig. 10, simplified into a series of linear segments closely matching the original curve. The stress-strain relationship of concrete in compression was assumed to be in accordance with the modified Hognestad's model [34], as demonstrated in Fig. 13. For concrete in tension, the stress-strain curve was assumed linear up to the tensile strength (equal to 4.1 MPa). For larger tensile strains, cracking occurs and a linear softening branch intersecting the strains axis at a strain equal to 0.001 is employed to reflect in an approximate manner the tension-stiffening effect in cracked concrete.

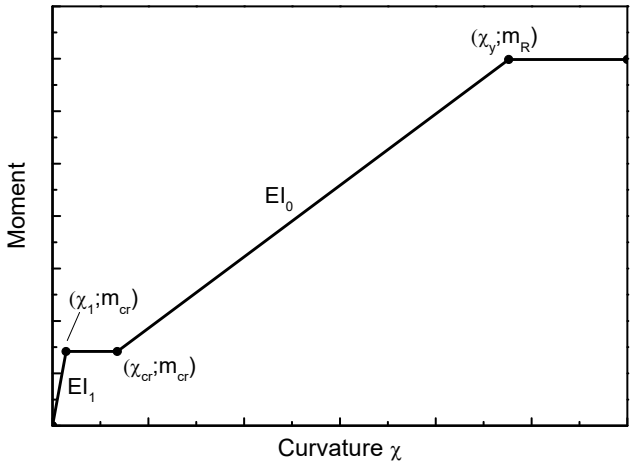

Fig. 12. Simplified quadrilinear moment-curvature relationship

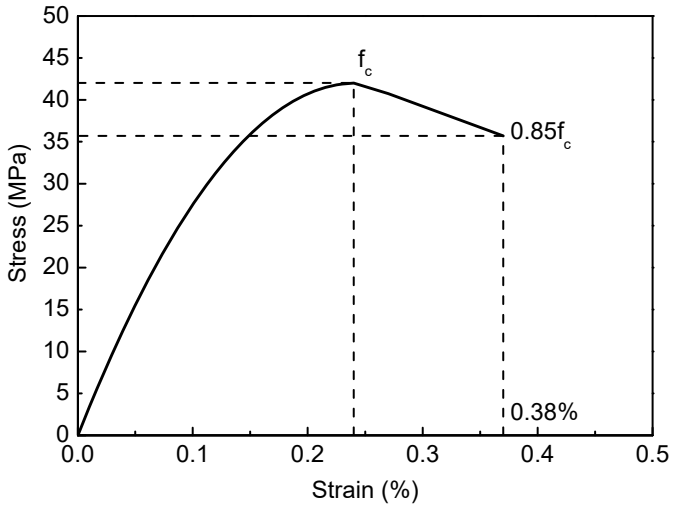

Fig. 13. Adopted stress-strain relationship for concrete in compression according to modified Hognestad's model

The moment-curvature curve was constructed following a numerical approach based on force equilibrium of a layered cross-section and strain compatibility, assuming that plane sections remain plane after deformations (a linear strain profile). Since the material and geometrical properties for slab specimens with the same longitudinal reinforcement ratio varied insignificantly, the moment-curvature relationships are presented in Fig. 14 for only two slabs (differing by the reinforcement ratio). The quadrilinear moment-curvature is plotted for comparison.

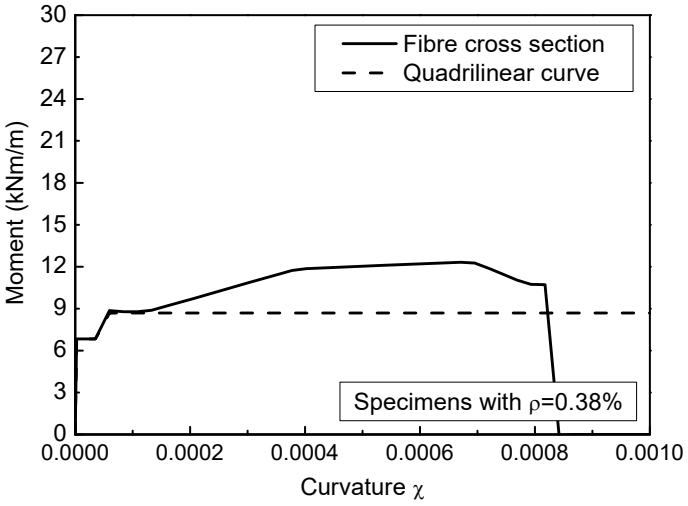

(a)

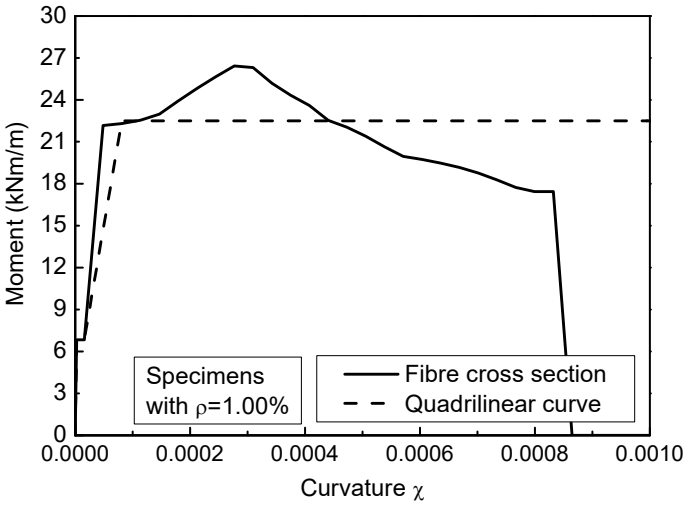

(b)

Fig. 14. Moment-curvature relationships considering the real nonlinear stress-strain curve of steel and simplified quadrilinear moment-curvatures; (a) specimens with ρ=0.38%; (b) specimens with ρ=1.00%.

As previously demonstrated in Table 3, Fig. 14 confirms that there is a significant increase of the resisting bending moment of the slab beyond the yielding bending moment. The moment-curvature relationships corresponding to the fiber cross-section approach are implemented into the CSCT in the analyses that follow.

4.3 Radius of the slab for the purpose of implementing CSCT

For the implementation of CSCT, it is necessary to determine the radius r_s of a circular slab that has the same flexural resistance V_{flex} as the experimentally tested square slab [35]. However, since the flexural capacity of the slab is determined by the equilibrium of slab sector elements and since the stress-strain relationships for concrete and steel are realistically modelled (see Section 4.2), fixing the value of r_s to have the same V_{flex} as the real slab specimen becomes challenging. For this reason, several alternatives are tested, resulting in different approaches for the consideration of the radius r_s, as described below:

- full implementation of the analytical model, with the moment-curvature relationships shown in Fig. 14 for fiber cross sections with steel and concrete in accordance with Fig. 10 and Fig. 13, respectively.

- full implementation of the analytical model but with simplified quadrilinear moment-curvature relationships as shown in Fig. 14, in accordance with Muttoni [21], using steel yield stress f_y in accordance with Fig. 10.
- simplified load-rotation relationship in accordance with Eq. (1), using $V_{flex} = V_{flex,u}$ from Table 3.

In the cases above, the radius is denoted as r_{sy} when its calculation is based on $V_{flex,y}$ and r_{su} when calculated based on $V_{flex,u}$. To calculate the radius r_s, the corresponding value of V_{flex} presented in Table 3 is equated with the V_{flex} calculated assuming a fan yield line mechanism of a circular slab with radius r_s supported on a circular column [35]. The radius of the column is taken equal to half the side dimension of the column's cross section. For the calculation of $r_{s,u}$, the same approach is followed in a first tentative, but then a correction factor is applied to the radius in order to obtain matching values of V_{flex}. This correction is necessary because the value of the tangential moments varies along the radius of the slab sector elements when the moment-curvatures from Fig. 14 with stress-strain curves from Fig. 10 and Fig. 13 are used.

Considering a quadrilinear moment-curvature (Fig. 12), the radius resulted in r_{sy}=1013 mm for the specimens with longitudinal reinforcement ratio equal to 0.38%, whereas for the specimens with 1.00% longitudinal reinforcement ratio the radius was r_{sy}=1029 mm. Calculating the moment capacity using the stress-strain curve of steel as described in Fig. 10 and concrete in accordance with Fig. 13, the radii resulted in r_{su}=1194 mm and r_{su}=1182 mm for specimens with longitudinal reinforcement ratio equal to 0.38% and 1.00%, respectively.

Also, it is necessary to know the radius r_q of the load application points. Using a similar test setup, Gosav et al. [36] showed that the radius r_q can be approximated by the radius of the inscribed circle to the square formed by the support lines. For the test setup of Fig.5, the radius is r_q=1700/2=850 mm.

For the simplified version of CSCT represented by Eq. (1), it is necessary to determine only r_s, which is assumed equal to the radius of the zero moment line (equal to r_q=850 mm in this case). In Eq. (1), the value of V_{flex} is entered manually (i.e., it is not derived by the equilibrium of sector elements) based on Table 3.

4.4 Results

The experimental results for specimens without shear reinforcement (US-0.38 and US-1.00) are compared with the predictions of CSCT in Fig. 15. Fig. 16 shows the results of the comparison between CSCT and the experiments for specimens with shear reinforcement (US-0.38-stud and US-1.00-stud). As discussed in Section 4.3, the load-rotation curve is constructed for several cases, considering different approaches for estimating the moment-curvature and different values of the radius of the equivalent circular slab.

Due to the relatively high amount of punching shear reinforcement used in the experimental campaign (Section 3), it was noticed that failure through the shear reinforcement is not relevant for the specimens under consideration. The same is true even if the diameter of the studs is reduced to account for the insufficient area of anchorage offered by the heads to develop full yield of the studs. The failure criterion for this failure mode (constructed in accordance with Ruiz and Muttoni [22]) is not shown in Fig. 16, for clarity of the figure, because it lays above the range of plotted values of the shear force.

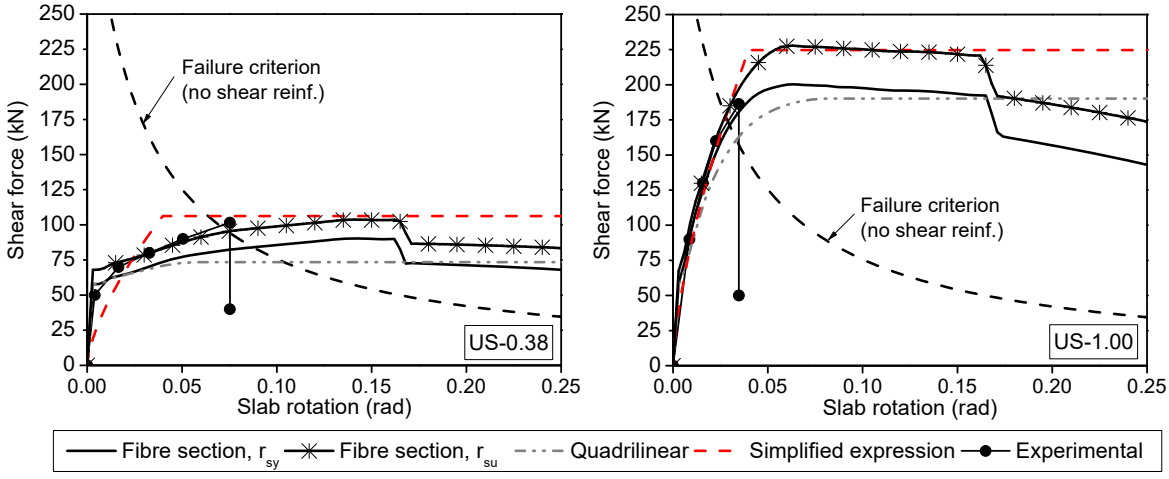

Fig. 15. Comparison of experimental results with CSCT for specimens without shear reinforcement

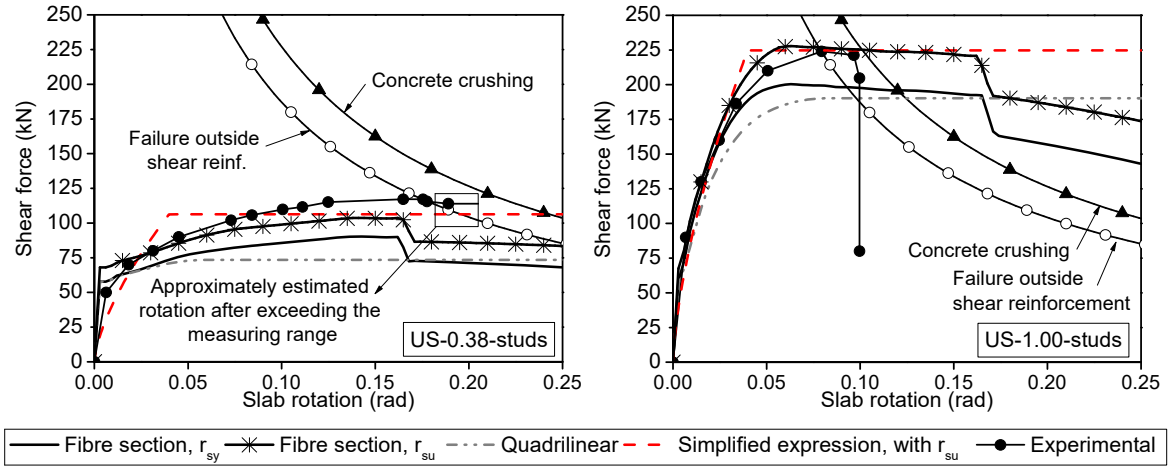

Fig. 16. Comparison of experimental results with CSCT for specimens with shear reinforcement

The failure loads predicted by four versions of the load-rotation curve considered as well as the experimental loads, V_{exp}, are summarized in Table 4.The failure loads calculated using a fiber section with radius r_{sy} and r_{su} are denoted as $V_{fiber,y}$ and $V_{fiber,u}$ respectively. The failure load in case the quadrilinear moment-curvature is used is denoted as $V_{quadrilinear}$. When the simplified approach is used, the failure load is denoted as $V_{simplified}$.

Table 4. Failure loads based on CSCT for different approaches of constructing the load-rotation curve

Specimen	V_{exp} (kN)	$V_{fiber,y}$ (kN)	$V_{fiber,u}$ (kN)	$V_{quadrilinear}$ (kN)	$V_{simplified}$ (kN)
US-0.38	101.6	84.0	95.3	73.7	106.3
US-0.38-stud	117.1	flexure*	flexure*	73.7	106.3
US-1.00	186.3	170.9	178.1	160.8	177.1
US-1.00-stud	224.0	198.1	226.9	190.4	224.7

*Flexural failure detected prior to punching. Punching prediction is therefore not reliable.

4.4.1 Failure modes and failure criteria

Referring to the load-rotation curves determined experimentally (Fig. 15 and Fig. 16), it is concluded that failure occurs reasonably close to the corresponding failure criteria of CSCT. This means that, regardless of the approach used to construct the load-rotation curve, the validity of the CSCT criteria is confirmed for the specimens under consideration. CSCT was

able to predict not only the ultimate loads but also the failure modes. According to Fig. 16, the specimens with shear reinforcement are predicted to fail outside the shear reinforced zone. This is the failure mode actually observed for these specimens (Section 3).

There is a slight underestimation by CSCT of the deformation capacity of the specimens with shear reinforcement (Fig. 16). This is already acknowledged in Ruiz and Muttoni [22], where it is argued that the failure criterion for failure outside the shear-reinforced zone adopts the conservative assumption of slab rotation concentrated in the region outside the critical shear crack (in this case, outside the shear-reinforced zone). The exact ultimate rotation of the specimen US-0.38-stud was not measured during the experiment, but this does not affect the discussion above. The ultimate rotation of this specimen was only marginally larger than the last measured value.

The fact that the experimental load-rotation curve intersects the corresponding failure criteria near the actual failure, means that, regardless of the discussions in the following section regarding the analytical construction of the load-rotation curve, a detailed nonlinear finite element analysis to construct the load-rotation curve of the slab can always be used in the framework of CSCT, as permitted in fib Model Code 2010 [37] for Level IV of Approximation. The following sections, however, shed light on limitations of the analytical approach described in [21] when used to construct the load-rotation curve.

4.4.2 Load-rotation curves for slab radius r_{sy}

Table 4 as well as Fig. 15 and Fig. 16 show that the predicted load-rotations curves for slab radius $r_{s,y}$ for the specimens with 1.00% longitudinal reinforcement ratio are closer to the experiment compared to those of the specimens with 0.38% reinforcement ratio. Comparing the load-rotation curves constructed based on different approaches in Fig. 15 and Fig. 16, it is noticed that modelling assumptions are more critical in the case of specimens US-0.38 and US-0.38-stud. In these specimens (specimens with low flexural reinforcement), the load-rotation curve constructed neglecting the post-yield behavior of the steel is relatively far from the experimental result. In specimen US-0.38, the ultimate load is severely underestimated (by nearly 27%) when the quadrilinear moment-curvature is used. Even with the moment-curvature constructed using a fiber section, there is an underestimation of the ultimate load by approximately 17% when the radius is taken equal to r_{sy}.

525 Referring to the lightly reinforced specimen with studs (US-0.38-stud), the ultimate load
526 remains underestimated (by nearly 37%) in case of a quadrilinear moment-curvature without
527 a strain hardening region of the steel reinforcement. More importantly, Fig. 16 shows that the
528 load-rotation curve is not captured well by the analytical models with the radius of the slab
529 equal to r_{sy}. A flexural failure, resulting in a softening of the load-rotation curve, is detected
530 for a slab rotation considerably lower than the rotation corresponding to the intersection with
531 the failure criteria. Since the deformed shape of the slab may change after a flexural failure,
532 the assumption of a conical deflected shape of the slab outside the critical shear crack is no
533 longer valid, and the results are therefore not reliable after this point. It is important to notice
534 that such a failure was not detected during the experimental campaign.

535 Looking at the predictions for specimens US-1.00 and US-1.00-stud in Fig. 15 and Fig. 16, it
536 is noticed that the situation is different from that described for the specimens with lower
537 longitudinal reinforcement ratio (equal to 0.38%). The load-rotation curves corresponding to
538 different approaches (but with radius $r_{s,y}$) are relatively close to each other and the behavior is
539 less depended on the assumptions related to steel's stress-strain relationship. Neglecting the
540 post-yield behavior of steel while using the quadrilinear moment-curvature leads to an
541 underestimation of the ultimate load of about 14% in specimen US-1.00 and of about 15% in
542 specimen US-1.00-stud. The predictions are better (8% and 12% underestimation of the
543 ultimate load respectively) when the actual stress-strain curve of steel is used (refer to Table
544 4).

545 The initial branch of the load-rotation curve is predicted reasonably well when the
546 experimental stress-strain relationship of steel is used (Fig. 10). However, the analytical
547 curves and the experimental ones diverge for larger slab rotations when the radius is
548 maintained equal to $r_{s,y}$.

549 For both levels of longitudinal reinforcement ratio, the curve corresponding to a simplified
550 quadrilinear moment-curvature relationship yields lower forces than the curve corresponding
551 to the exact moment-curvature relationship. This difference is expected to be smaller in
552 normally reinforced specimens when steel with a more pronounced yielding plateau is used
553 (unlike the steel shown in Fig. 10). Two specimens reported in Guandalini et al. [28] had a
554 longitudinal reinforcement ratio of 0.33% and thickness 250 mm, but one of the specimens
555 had steel without a clear yielding plateau. No significant difference was observed in the

behavior of the two specimens, indicating that the effect of the longitudinal reinforcement steel post-yield behavior is more pronounced in thin lightly reinforced slabs.

4.4.3 Load-rotation curves for slab radius r_{su}

This section presents the analysis results assuming a hypothetical slab radius equal to r_{su}, calculated on the basis of $V_{flex,u}$. Fig. 15 and Fig. 16 indicate that this approach is suitable for the specimens under consideration. Using r_{su} leads to a load-rotation curve that is able to track the entire experimental curve. However, the approach worked better for specimens with 1.00% longitudinal reinforcement ratio.

Table 4 shows that the predictions of the model considering a fiber section and slab radius r_{su} result in ultimate loads that are closer to V_{exp} compared to alternatives assuming a radius r_{sy}. The failure load prediction was underestimated by 6% in specimen US-0.38, by only 4% in specimen US-1.00 and it was slightly overestimated by nearly 1% in US-1.00-stud.In specimen US-0.38-studs, a flexural failure before punching is predicted, the same as in case of radius $r_{s,y}$. Nonetheless, the predicted flexural failure is relatively close to the failure criterion for punching outside the shear-reinforced zone.

Looking at the load-rotation curve corresponding to the simplified version of CSCT with radius $r_{s,u}$, it is noticed that it deviates significantly for specimens with low longitudinal reinforcement ratio. On the other hand, it is reasonably close to the experimental curve in specimens with 1.00% longitudinal reinforcement ratio. It should be noted that the effect of post-yield stress-strain relationship of steel is already included in an approximate manner in the simplified load-rotation curve through the use of $V_{flex,u}$ in Eq. (1).

Although the failure loads predicted using the simplified approach are close to the experimental loads (Table 4), this approach should be considered with caution in thin lightly reinforced flat slabs because it does not follow the experimental curve closely for each value of the slab's rotation.

5 Further verifications and discussion

5.1 Re-examination of tests from the literature

In Section 4 it was shown that the approach to analytically construct the load-rotation curve that is closer to the experimental results of the specimens presented in Section 3 is to consider a radius of the slab equal to $r_{s,u}$ and to explicitly take into account the nonlinear behavior of concrete and steel. Further verification of the assumptions employed in Section 4 with specimens from the literature is not straightforward, because the information required is seldom provided in the literature (i.e., the complete stress-strain curve of steel, slab rotations as a function of the load, *etc*.).

Tests on thin and lightly reinforced flat slabs presented in Guandalini et al. [28] are re-examined in this Section. For these specimens, it was possible to find relevant additional information in [38]. Although a numerical model considering strain hardening was used in [38] for the derivation of the analytical load-rotation curves, a direct comparison with a model that neglects strain hardening was not found. As already mentioned in Section 2.2, the thin lightly reinforced specimens of Guandalini et al. [28] are named PG-8 and PG-9. The specimens of Guandalini et al. [28] had a ratio f_u/f_y equal to 1.12 and a clear yielding plateau in the stress-strain curve of steel. In contrast, the specimens tested in the current study, presented in Section 3, had a higher ratio f_u/f_y equal to 1.56 and a short yielding plateau of steel (Fig. 10). Furthermore, the greater thickness in the specimens of Guandalini et al. [28] means a less ductile behavior and less excursion into the post-yield region of the stress-strain curve of steel. For all these reasons, the influence of the stress-strain relationship of steel is expected to be milder in specimens of Guandalini et al. [28]. Fig. 17 presents a comparison of the analytically derived load-rotation curves based on the approach described in Section 4 for specimens PG-8 and PG-9. The strain at the onset of strain hardening and strain at steel rupture was not found for specimens PG-8 and PG-9, but the information provided in [38] for other specimens tested in the same experimental campaign was assumed to apply for these two specimens as well.

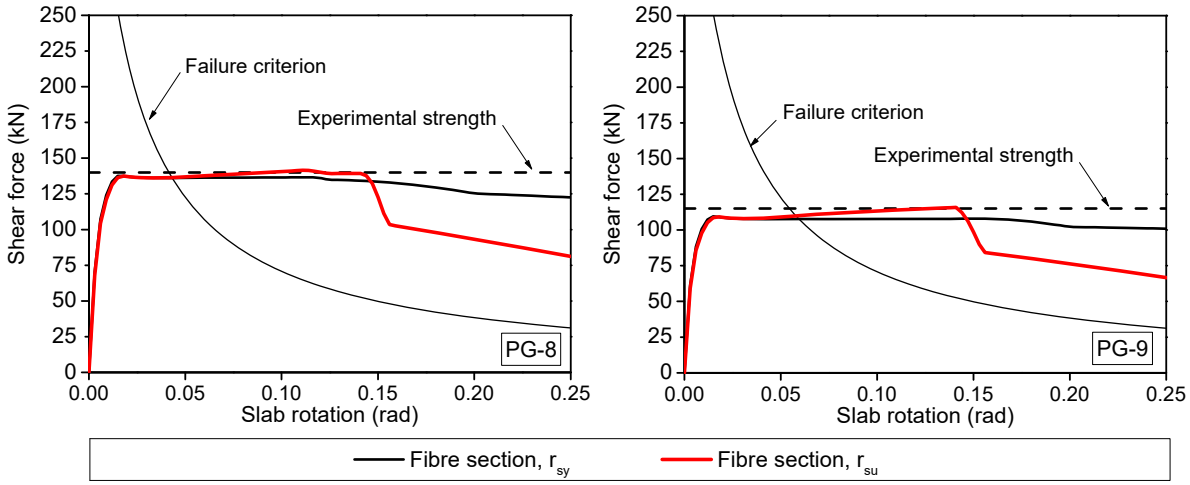

608

609 Fig. 17. Role of steel stress-strain curve in specimens of Guandalini et al. [28]

610 Fig. 17 confirms that the stress-strain curve of steel does play a role in the analytical
611 derivation of the load-rotation curve for the specimens of Guandalini et al. [28], although
612 small and with a negligible effect on the load capacity prediction in this case. For the reasons
613 stated above, the behavior is not affected as much as in the case of specimens presented in
614 this paper in Section 3. The range of values in the axes in Fig. 17 was intentionally kept the
615 same as in Fig. 15 and Fig. 16. A comparison of Fig. 17 with Fig. 15 and Fig. 16 shows that
616 specimens US-0.38 and US-0.38-studs failed for larger slab rotations compared to PG-8 and
617 PG-9. This observation further indicates that the thinner the slab and the shorter the yielding
618 plateau of the steel, the more pronounced is the effect of the post-yield stress-strain curve of
619 steel.

620 **5.2 Finite Element Analysis**

621 A Finite Element Analysis (FEA) was conducted to further analyze the role of the stress-
622 strain curve of steel in thin lightly reinforced flat slabs. The analysis was conducted using the
623 commercial software ABAQUS [39]. A quarter of the specimen US-0.38 was modelled, as
624 demonstrated in Fig. 18, to benefit from the symmetrical conditions. Two versions of the
625 model were analyzed, with the only difference between them being the stress-strain curve of
626 steel used for the reinforcing bars.

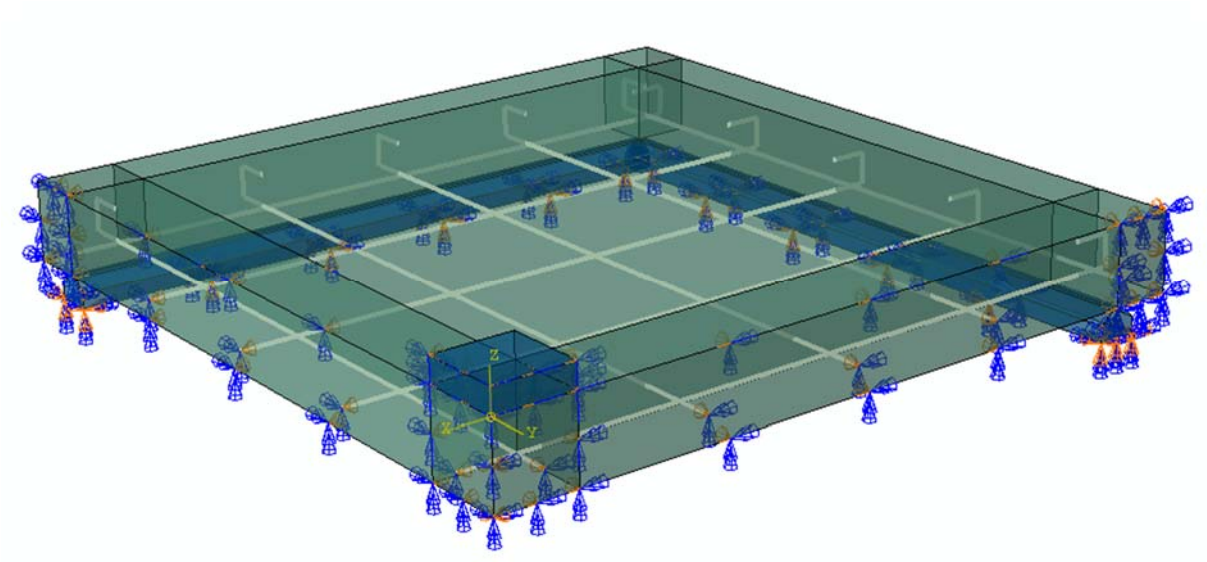

Fig. 18. Numerical model of the specimen US-0.38

The recommendations from Genikomsou and Polak [40] were followed closely since they directly refer to the problem of punching shear in flat slabs. To model concrete, the Concrete Damaged Plasticity (CDP) model was used, with a dilation angle equal to 40 degrees, eccentricity 0.1, the ratio between biaxial and uniaxial concrete strength equal to 1.16 and a shape factor of the yield surface equal to 0.667 [40]. The analysis was conducted under static loading, with a viscosity parameter equal to 5×10^{-5}. This parameter was chosen sufficiently large to ensure convergence of the analysis when localized cracking occurs. This viscosity regularization is at the expense of the accuracy of the determination of the punching shear failure point [41]. For the purposes of this study, however, the main interest is on the effect of steel's stress-strain curve on the load-displacement curve, and the discussion is valid regardless of the load level in which punching shear failure occurs. Tension and compression damages were neglected because these factors are most relevant in cases of cyclic loading [40, 41].

The uniaxial concrete and steel properties already described in Section 4 were used, with the difference that the tensile behavior of concrete was modelled as described in [40], with the fracture energy calculated in accordance with Model Code 2010 [37] and a tensile strength reduced to 50% of the theoretical value to account for early cracking that occurred in the specimen. This reduction of the tensile strength does not affect the post-yield load-rotation curve. In one model, a hypothetical bilinear linear perfectly-plastic stress-strain curve of steel

with yield stress equal to f_y was used, while maintaining all the other model parameters unchanged.

The loading plate and the supports were modelled using steel elements with dimensions as in the experimental test. Symmetry boundary conditions were imposed along the axes of symmetry of the model (Fig. 18). A contact interaction was defined to accurately model the support conditions of the slab, allowing uplift of the corners. The cylindrical supports were substituted with prismatic supports with a small enough contact area to avoid large concentration of stresses and no friction. The slab was modelled with brick elements (5 elements along the depth of the slab, resulting in finite elements with the size the same as in [40]). The reinforcement bars were modelled as embedded truss elements with the perfect bond. The choices above (e.g., regarding mesh size and energy of fracture) were based on a series of preliminary analyses, keeping in mind the purpose and limitations of the presented model as described earlier.

Fig. 19 demonstrates that the model worked as intended. The deformed shape of Fig. 19a for a maximum deflection of 60 mm shows that the boundary conditions were modelled properly because uplift of the corners of the specimen comparable with the experiment was detected (Fig. 8). The crack pattern demonstrated in Fig. 19b matches reasonably well with the flexural crack pattern observed during the test (Fig.9). More importantly, Fig. 19a and Fig. 19b support the assumed yield line pattern used throughout this study to calculate the flexural capacity V_{flex} of the specimens (Fig. 11).

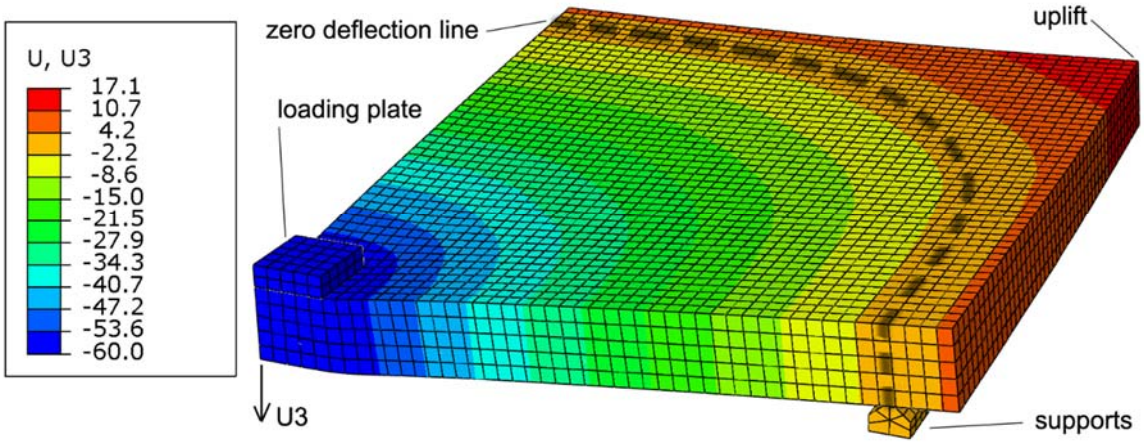

(a)

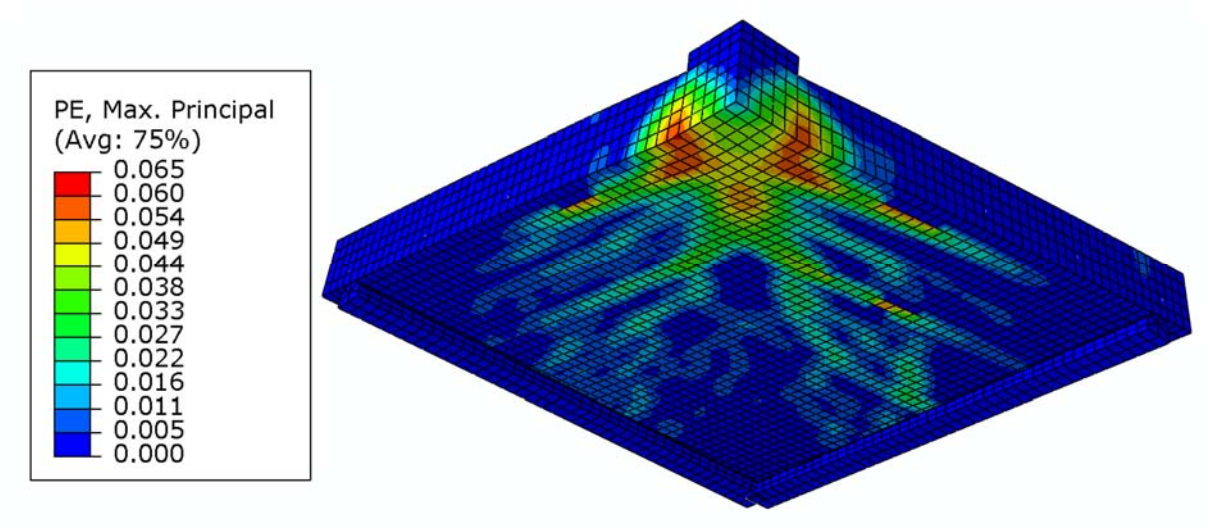

(b)

Fig. 19. FEA results; (a) deformed shape for a maximum deflection of 60 mm; (b) cracking pattern for a maximum deflection of 60 mm

The FEA results are compared in Fig. 20 with the experiment and with the predicted loads $V_{flex,y}$ and $V_{flex,u}$ from Table 4.The results in Fig. 20 confirm the role of the post-yield stress-strain curve of steel in the behavior of the 100 mm thick specimens with reinforcement ratio equal to 0.38%. The curve corresponding to the model with elastic-perfectly plastic steel (without strain hardening) is further away from the experiment compared to the other model that realistically models steel.

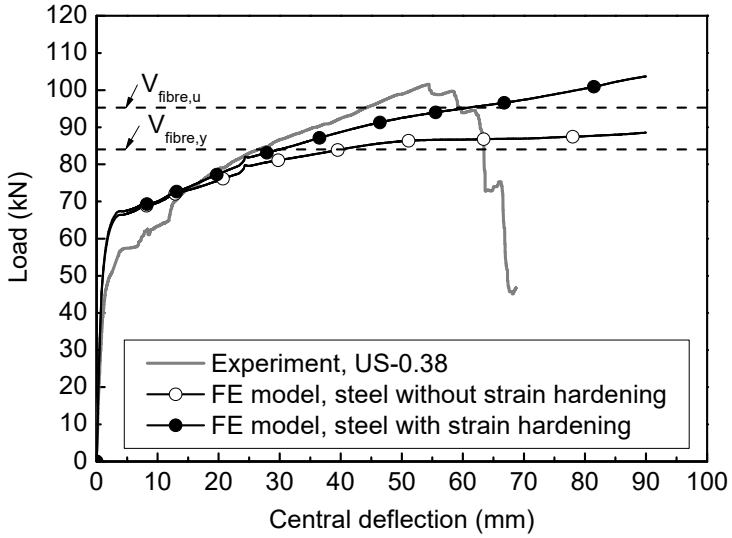

Fig. 20. Comparison of the FEA and experimental results

682 ### 5.3 Comparison with "flexure-induced punching" based on Ghali and Gayed

683 As previously described, all specimens except US-1.00 exhibited significant flexural yielding
684 before their ultimate failure, which can be characterised as "flexure-induced punching"[12].
685 A comparison of the experimental results with the provisions of Ghali and Gayed [12] for this
686 type of failure is presented in this section.

687 According to Ghali and Gayed [12], the current ACI 318 [16] punching shear provisions need
688 to be supplemented such that premature flexure-induced punching is effectively avoided,
689 especially in lightly reinforced flat slabs which have been shown [33] to fail for loads lower
690 than the prediction of the ACI 318 code. A simple solution to this issue according to Ghali
691 and Gayed [12] is to ensure that the amount of flexural reinforcement in the vicinity of the
692 column exceeds a minimum value corresponding to the formation of a yield line mechanism
693 when the slab's reaction on the column is equal to the punching shear resistance of the flat
694 slab. For the specimens presented in this paper, this means that a comparison between the
695 punching shear resistance in accordance with ACI 318 [16], V_{ACI}, and the flexural capacity
696 already presented in Table 3 (based on yield-line theory) is necessary.

697 The punching shear resistances in accordance with ACI 318 [16] are summarized in Table 5,
698 for failure through shear reinforcement ($V_{s,ACI}$) and failure outside the shear-reinforced zone
699 ($V_{o,ACI}$). The governing failure mode is then denoted as V_{ACI} in Table 5.For specimens
700 without shear reinforcement, V_{ACI} is directly calculated as the punching shear resistance
701 considering a control perimeter located at a distance $d/2$ from the face of the column.
702 Calculations are performed considering strength reduction factors equal to 1.0.

703 Table 5. Assessment of flexure-induced punching based on Ghali and Gayed [12]

Specimen	$V_{s,ACI}$ (kN)	$V_{o,ACI}$ (kN)	V_{ACI} (kN)	$V_{flex,y}$ (kN)	$V_{flex,u}$ (kN)	$V_{ACI}/V_{flex,u}$
US-0.38	N/A*	N/A	169.5	73.7	106.3	1.59
US-0.38-stud	333.9	283.2	283.2	73.7	106.3	2.66
US-1.00	N/A	N/A	167.3	190.4	224.7	0.74
US-1.00-stud	335.9	284.9	284.9	190.4	224.7	1.27

704 *N/A – not applicable

705 Table 5 shows that, according to ACI 318 [16], the governing shear failure mode is punching
706 outside the shear-reinforced zone for the specimens with studs. For all the specimens that

707 experienced flexure-induced punching (that is, all specimens except US-1.00), the load
708 corresponding to flexural failure (V_{flex}, both considering and neglecting strain hardening of
709 flexural reinforcement) is lower than the punching shear resistance according to ACI 318
710 [16]. On the contrary, V_{ACI} is smaller than $V_{flex,y}$ and $V_{flex,u}$ in case of US-1.00, and punching
711 failure occurred before significant flexural yielding in this specimen (refer to Fig.7 and Fig.
712 15).

713 The analysis above indicates that the rather simple approach proposed by Ghali and Gayed
714 [12] predicts reasonably well the overall behavior of thin lightly reinforced flat slabs. A
715 significant improvement of the load carrying capacity of the specimens (except US-1.00)
716 would be achieved by increasing the amount of flexural reinforcement such that $V_{ACI} = V_{flex,u}$
717 (refer to the last column in Table 5).

718 **5.4 Considerations for practice**

719 Flat slabs as thin and as lightly reinforced as the ones described in this paper may not be
720 much usual in practice. However, a few possible extreme cases referring to existing structures
721 were listed in Section 1. Furthermore, with the modern developments in the concrete
722 technology having ultra-high performance concrete, and new developments to have high
723 strength steel rebars without losing ductility, thin and lightly reinforced flat slabs can find
724 their use in the design of new structures. Verification of the CSCT failure criteria will be
725 necessary in this case due to the changes in concrete properties, but the discussions above
726 regarding the analytical construction of the load-rotation curve can be useful.

727 In practice, assuming an elastic-perfectly plastic relationship for steel reinforcement (without
728 a strain hardening region) will normally lead to an underestimation of the flexural load
729 carrying capacity, which is normally on the safe side. However, the anticipated failure mode
730 can change in some cases from flexure to punching (brittle). A simple check as demonstrated
731 in Section 5.3 can be useful in determining the failure mode, whereas CSCT can be used for a
732 detailed design. Nonetheless, this paper showed that the significant influence of the post-yield
733 regime of steel can be expected in practice in cases where the slab is very thin and when the
734 yielding plateau of steel is short. In these cases, researchers and practitioners are suggested to
735 be cautious in applying the simplified approaches for the construction of the load-rotation
736 curves in the framework of CSCT.

6 Conclusions

The concentric monotonic punching shear tests of four thin flat slab specimens were described and analysed in this paper in the light of Critical Shear Crack Theory (CSCT). Two of the specimens were lightly reinforced (ρ=0.38%), whereas two other specimens had a reinforcement ratio of 1.00%. For each reinforcement ratio, one specimen without shear reinforcement and one with shear studs were tested. The main conclusions are summarized below:

1. The ultimate failure mode in all tested specimens was punching shear. The behavior of the specimens was highly influenced by the employed flexural and shear reinforcement.
2. The post-cracking behavior of the tested slabs was significantly influenced by the flexural reinforcement ratio. After cracking, the stiffness of the specimens with a reinforcement ratio of 0.38% was much lower than that of the specimens with a reinforcement ratio of 1.00%. In specimens with relatively large deformations, this behavior was considerably affected by the strain-hardening region in the stress-strain curve of steel reinforcement.
3. The introduction of shear reinforcement led to a more ductile behavior of the specimens, regardless of the amount of flexural reinforcement.
4. The failure load was reasonably close to the prediction of CSCT and the failure modes were correctly predicted by CSCT. This indicates that the failure criteria of CSCT are applicable also to the special case of thin lightly reinforced flat slabs;
5. The load-rotation curve and the failure points of the specimens with 1.00% longitudinal reinforcement ratio were predicted by CSCT better than those of the specimens with 0.38% reinforcement ratio.
6. While it was shown that CSCT can be applied to thin lightly reinforced flat slabs, attention is drawn throughout the paper to a number of issues that need to be taken into consideration while analysing such slabs. It was shown that the stress-strain relationship of steel needs to be taken into account explicitly when large deformations of the slab are expected (as in the case of lightly reinforced flat slabs), especially when steel does not exhibit a clear yielding plateau. The versatility of CSCT to adapt to this scenario was demonstrated by the use of a fiber section to describe the moment-curvature behavior of the slab using nonlinear material properties.
7. The simplified formulation of CSCT (Eq. (1)) considering the strain hardening effect was successful in predicting reasonably well the ultimate load of the specimens, but the load-

rotation curve deviated significantly from the experiment for lower load levels in specimens with a longitudinal reinforcement ratio of 0.38%.

Acknowledgments

The Department of Civil Engineering of Isfahan University of Technology (IUT) is greatly appreciated for its valuable support in providing the test facilities in the structural laboratory. Furthermore, the financial support of research Deputy of IUT for providing the test materials is deeply appreciated.

Notations

b_0	control perimeter, taken at a distance $d/2$ from the column
c	slab side length
d	effective depth of the slab
d_g	maximum aggregate size
d_{g0}	reference aggregate size
E_s	modulus of elasticity of steel
f_c	compressive strength of concrete
f_{ck}	characteristic compressive strength of concrete at 28 days
f_y	steel yield stress
f_u	ultimate steel stress considering strain hardening
k	coefficient used in punching provisions of Eurocode 2
l_l	distance between the supports
l_s	slab side length
l_{up}	length of support facing uplift of slab
r_c	radius of the column
r_q	radius of the load application points
r_s	radius of the slab

r_{sy}	radius of the slab when calculated based on $V_{flex,y}$
r_{su}	radius of the slab when calculated based on $V_{flex,u}$
r_0	radius of the critical crack
v_c	punching shear resistance (stress) of slab without shear reinforcement
v_{min}	minimum shear resistance (stress) of slab without shear reinforcement
V	applied shear force
V_{ACI}	punching shear strength in accordance with ACI 318
V_{exp}	experimental load
$V_{fiber,y}$	failure load calculated using a fiber section with radius r_{sy}
$V_{fiber,u}$	failure loads calculated using a fiber section with radius r_{su}
V_{flex}	flexural strength of the slab
$V_{flex,y}$	flexural capacity of the slab assuming steel yield stress
$V_{flex,u}$	ultimate flexural capacity assuming strain hardening
$V_{o,ACI}$	punching shear strength for failure outside the shear-reinforced zone
$V_{quadrilinear}$	failure load in case the quadrilinear moment-curvature is used
$V_{simplified}$	failure load when the simplified approach is used
$V_{s,ACI}$	punching shear strength for failure through shear reinforcement
α_s	coefficient used in punching provisions of ACI 318 for different columns
β	ratio of long to short sides of the column
γ_c	partial factor for concrete
λ	multiplier factor used by Ruiz and Muttoni for shear reinforcement
ρ	flexural steel reinforcement ratio
ρ_y	flexural reinforcement ratio related to steel bonded in y-direction
ρ_z	flexural reinforcement ratio related to steel bonded in z-direction
ψ	slab rotation

Funding

This research did not receive any specific grant from funding agencies in the public, commercial, or not-for-profit sectors.

References

[1] Stein T, Ghali A, Dilger W. Distinction between punching and flexural failure modes of flat plates. ACI Struct J. 2007;104(3):357-65.

[2] Mortin JD, Ghali A. Connection of flat plates to edge columns. Structural Journal. 1991;88(2):191-8.

[3] Ricker M, Häusler F. European punching design provisions for double-headed studs. Proceedings of the Institution of Civil Engineers-Structures and Buildings. 2014;167(8):495-506.

[4] Vollum R, Abdel-Fattah T, Eder M, Elghazouli A. Design of ACI-type punching shear reinforcement to Eurocode 2. Magazine of Concrete Research. 2010;62(1):3-16.

[5] Meisami MH, Mostofinejad D, Nakamura H. Punching shear strengthening of two-way flat slabs using CFRP rods. Compos Struct. 2013;99:112-22.

[6] Meisami MH, Mostofinejad D, Nakamura H. Punching shear strengthening of two-way flat slabs with CFRP grids. J Compos Constr. 2013;18(2):04013047.

[7] Meisami MH, Mostofinejad D, Nakamura H. Strengthening of flat slabs with FRP fan for punching shear. Compos Struct. 2015;119:305-14.

[8] Inácio MM, Ramos AP, Faria DM. Strengthening of flat slabs with transverse reinforcement by introduction of steel bolts using different anchorage approaches. Eng Struct. 2012;44:63-77.

[9] Ebead U, Marzouk H. Fiber-reinforced polymer strengthening of two-way slabs. ACI Struct J. 2004;101(5):650-9.

[10] Michel L, Ferrier E, Agbossou A, Hamelin P. Flexural stiffness modeling of RC slab strengthened by externally bonded FRP. Compos Part B: Eng. 2009;40(8):758-65.

[11] Elstner RC, Hognestad E. Shearing strength of reinforced concrete slabs. Journal Proceedings. 1956;53(7):29-58.

[12] Ghali A, Gayed RB. Universal Design for Punching Resistance of Concrete Slabs. ACI Struct J. 2019;116(1):207-12.

[13] Criswell M. Static and dynamic response of reinforced concrete slab-column connections. Special Publication. 1974;42:721-46.
[14] Abbasi M, Baluch M, Azad A, Rahman HA. Nonlinear finite element modeling of failure modes in RC slabs. Computers & structures. 1992;42(5):815-23.
[15] Afhami S, Alexander SD, Simmonds SH. Strip model for capacity of slab-column connections. Structural Engineering Report No 223, University of Alberta. 1998.
[16] Building code requirements for structural concrete (ACI 318-14). Farmington Hills, MI, USA: ACI Committee 318; 2014.
[17] Eurocode 2. Design of concrete structures. —Part 1-1: General Rules and Rules for Buildings, CEN, EN 1992-1-1, Brussels, Belgium, 2004.
[18] Fédération Internationale du Béton (fib). fib Model Code for Concrete Structures 1990. Thomas Telford Ltd., 1993.
[19] Muttoni A, Schwartz J. Behavior of beams and punching in slabs without shear reinforcement. IABSE colloquium: IABSE Colloquium; 1991.
[20] Kinnunen S, Nylander H. Punching of concrete slabs without shear reinforcement: Elander; 1960.
[21] Muttoni A. Punching shear strength of reinforced concrete slabs without transverse reinforcement. ACI Struct J. 2008;105(4):440-50.
[22] Fernández Ruiz M, Muttoni A. Applications of the critical shear crack theory to punching of R/C slabs with transverse reinforcement. ACI Struct J. 2009;106(4):485-94.
[23] Clément T, Ramos AP, Fernández Ruiz M, Muttoni A. Design for punching of prestressed concrete slabs. Structural Concrete. 2013;14(2):157-67.
[24] Clément T, Ramos AP, Ruiz MF, Muttoni A. Influence of prestressing on the punching strength of post-tensioned slabs. Eng Struct. 2014;72:56-69.
[25] Faria DM, Einpaul J, Ramos AM, Ruiz MF, Muttoni A. On the efficiency of flat slabs strengthening against punching using externally bonded fiber reinforced polymers. Constr Build Mater. 2014;73:366-77.
[26] Lapi M, Fernandes H, Orlando M, Ramos A, Lúcio V. Performance assessment of flat slabs strengthened with a bonded reinforced-concrete overlay. Magazine of Concrete Research. 2017;70(9):433-51.
[27] Lapi M, Ramos AP, Orlando M. Flat slab strengthening techniques against punching-shear. Eng Struct. 2019;180:160-80.
[28] Guandalini S, Burdet O, Muttoni A. Punching tests of slabs with low reinforcement ratios. ACI Struct J. 2009;106(1):87-95.

[29] Einpaul J, Bujnak J, Fernández Ruiz M, Muttoni A. Study on influence of column size and slab slenderness on punching strength. ACI Struct J. 2016;113(1):135-45.
[30] ASTM A1044. Standard specification for steel stud assemblies for shear reinforcement of concrete. American Society for Testing and Materials (ASTM); 2010.
[31] ASTM C39/C 39M-04a. Standard test method for compressive strength of cylindrical concrete specimens. American Society for Testing and Materials (ASTM); 2005.
[32] Rankin G, Long A. Predicting the punching strength of conventional slab-column specimens. Proceedings of the Institution of Civil Engineers. 1987;82(2):327-46.
[33] Gayed RB, Peiris C, Ghali A. Flexure-induced punching of concrete flat plates. Special Publication. 2017;315:73-99.
[34] Hognestad E, Hanson NW, McHenry D. Concrete stress distribution in ultimate strength design. Journal Proceedings. 1955;52(12):455-80.
[35] Lips, S., Punching of flat slabs with large amounts of shear reinforcement (Doctoral dissertation), Lausanne: École Polytechnique Fédérale de Lausanne. 2012. .
[36] Gosav AV, Kiss ZI, Oneţ T, Bompa DV. Failure assessment of flat slab-to-column members. Magazine of Concrete Research. 2016;68(17):887-901.
[37] Fédération Internationale du Béton (fib). fib Model Code for Concrete Structures 2010. s.l.:Ernst & Sohn, 2013.
[38] Guandalini S. Poinçonnement symétrique des dalles en béton armé, Ph.D. thesis. Lausanne, EPFL; 2006.
[39] ABAQUS Analysis user's manual, version 6.16, Dassault Systems Simulia Corp., 2016.
[40] Genikomsou AS, Polak MA. Finite element analysis of punching shear of concrete slabs using damaged plasticity model in ABAQUS. Eng Struct. 2015;98:38-48.
[41] Wosatko A, Pamin J, Polak MA. Application of damage–plasticity models in finite element analysis of punching shear. Computers & Structures. 2015;151:73-85.